Research Square

Preprints are preliminary reports that have not undergone peer review.
They should not be considered conclusive, used to inform clinical practice,
or referenced by the media as validated information.

Fungal hyphae instigate non-canonical inflammatory cell death in macrophages

Axel Dietschmann

axel.dietschmann@leibniz-hki.de

Leibniz Institute for Natural Product Research and Infection Biology – Hans-Knöll-Institute (Leibniz-HKI)
https://orcid.org/0000-0002-0598-9714

Laszlo Musiejovsky

Medical University of Vienna https://orcid.org/0009-0002-9238-4752

Thomas Krüger

Leibniz Institute for Natural Product Research and Infection Biology (Leibniz-HKI)
https://orcid.org/0000-0001-8984-3853

Collins Bohaen

Radboud University Medical Center

Sude Dinçer

Leibniz Institute for Natural Product Research and Infection Biology – Hans-Knöll-Institute (Leibniz-HKI)

Fay Bruggeman

Leibniz Institute for Natural Product Research and Infection Biology – Hans-Knöll-Institute (Leibniz-HKI)

Ceren Oktay

Leibniz Institute for Natural Product Research and Infection Biology - Hans-Knöll-Institute (Leibniz-HKI)
https://orcid.org/0009-0008-5496-8582

Marisa Valentine

Leibniz Institute for Natural Product Research and Infection Biology – Hans-Knöll-Institute (Leibniz-HKI)

Maximilian Himmel

Department of Microbial Pathogenicity Mechanisms, Leibniz Institute for Natural Product Research and Infection Biology - Hans Knoell Institute (HKI), Jena, Germany

Stefan Wirtz

University of Erlangen-Nuremberg https://orcid.org/0000-0001-6936-7431

Eicke Latz

University of Bonn

Jürgen Ruland

Technical University of Munich

Olaf Kniemeyer

Leibniz Institute for Natural Product Research and Infection Biology (HKI) https://orcid.org/0000-0002-9493-6402

Vinod Kumar
Radboud University Medical Center, Nijmegen
Gernot Schabbauer
Medical University of Vienna
Mark Gresnigt
Leibniz Institute for Natural Product Research and Infection Biology - Hans Knöll Institute
https://orcid.org/0000-0002-9514-4634

Article

Keywords: Hyphoptosis, Filamentous morphology, Candidiasis, Candida albicans, Neutrophil activation, Trained immunity, Immunotherapy

Posted Date: March 17th, 2026

DOI: https://doi.org/10.21203/rs.3.rs-8296333/v1

License: This work is licensed under a Creative Commons Attribution 4.0 International License.
Read Full License

Additional Declarations: There is **NO** Competing Interest.

Fungal hyphae instigate non-canonical inflammatory cell death in macrophages

Axel Dietschmann[1,*], Laszlo Musiejovsky[2], Thomas Krüger[3], Collins K. Boahen[4], Sude Dinçer[1], Fay Bruggeman[1], Ceren Oktay[1], Marisa Valentine[5], Maximilian Himmel[1], Stefan Wirtz[6], Eicke Latz[7], Jürgen Ruland[8], Olaf Kniemeyer[3], Vinod Kumar[4,9], Gernot Schabbauer[2], Mark S. Gresnigt[1,10,*]

Affiliations

[1]Junior Research Group Adaptive Pathogenicity Strategies, Leibniz Institute for Natural Product Research and Infection Biology – Hans-Knöll-Institute (Leibniz-HKI), Beutenbergstraße 11a 07745,

[2]Institute of Vascular Biology and Thrombosis Research, Center for Physiology and Pharmacology, Medical University of Vienna, Vienna, Austria; Christian Doppler Laboratory for Arginine Metabolism in Rheumatoid Arthritis and Multiple Sclerosis, Vienna, Austria

[3]Department of Molecular and Applied Microbiology, Leibniz Institute for Natural Product Research and Infection Biology – Hans Knöll Institute (HKI), Jena, Germany

[4]Department of Internal Medicine and Radboud Institute of Molecular Life Sciences (RIMLS), Radboud University Medical Center, Nijmegen, 6525 HP, the Netherlands

[5]Department of Microbial Pathogenicity Mechanisms, Leibniz Institute for Natural Product Research and Infection Biology – Hans Knöll Institute (HKI), Jena, Germany

[6]Deutsches Zentrum für Immuntherapie (DZI), Friedrich-Alexander University Erlangen-Nürnberg (FAU) and Universitätsklinikum Erlangen, Germany; Department of Internal Medicine 1, Friedrich-Alexander University Erlangen-Nürnberg (FAU) and Universitätsklinikum Erlangen, Erlangen, Germany

[7]Institute of Innate Immunity, University Hospital, University of Bonn, Bonn, Germany.

[8]Institute of Clinical Chemistry and Pathobiochemistry, School of Medicine and Health, Center for Translational Cancer Research (TranslaTUM), Munich, Germany; German Cancer Consortium (DKTK), partner site Munich, Germany; German Center for Infection Research (DZIF), partner site Munich, Germany

[9]Nitte (Deemed to Be University), Medical Sciences Complex, Nitte University Centre for Science Education and Research (NUCSER), Deralakatte, Mangalore, 575018, India

[10]Lead contact

***Correspondence:**

axel.dietschmann@leibniz-hki.de

mark.gresnigt@leibniz-hki.de

Adolf-Reichwein-Straße 23, 07749, Jena, Germany

Short title: Hyphoptosis shapes innate immune-fungal interactions

Abstract

Fungal pathogens annually claim around 1.5 million lives, for which they are increasingly recognized as a threat to human health. Protective antifungal immunity centrally involves innate phagocytes. Many fungi switch morphologies to overcome defences and cause disease. Filamentation, particularly for the polymorphic fungus *Candida albicans*, is tightly connected with tissue invasion, lytic escape from within phagocytes, toxin production, and pyroptosis. Current infection models often disregard the interactions between extracellular hyphae and phagocytes. Yet, here we reveal a previously overlooked mechanism of macrophage cell death during fungal infection. Upon hyphal recognition, macrophages undergo host-regulated, non-pyroptotic, inflammatory death ("hyphoptosis") that stimulates vigorous neutrophil responses. We identified C-type lectin, integrin, PI3K and ROS signalling driving this macrophage-specific cell death, which can be alleviated by immunotherapeutic macrophage rewiring with GM-CSF or IL-4. Genetic variation in the pathway associated with candidemia, proposing that dysregulation of hyphoptosis impacts human susceptibility to life-threatening invasive candidiasis.

Key words:

Hyphoptosis, Filamentous morphology, Candidiasis, *Candida albicans*, Neutrophil activation, Trained immunity, Immunotherapy

Introduction

Human fungal infections are recognized as major global health issue by the WHO and estimated to be responsible for over 1.5 million annual deaths.[1, 2] The WHO highlights eleven fungal species as critical or high priority pathogens, requiring further research to minimize their threat to human health.[1] Nearly all those fungi perform infection-relevant morphological switches and more than half of them commonly form filamentous hyphae during infection.[3-11] A prime example of a critical group pathogen that uses hyphal growth to cause disease, is *Candida albicans*.[3, 12] *C. albicans* is a major cause for 1) a vast number of mucocutaneous infections, particularly vulvovaginal candidiasis and 2) invasive candidiasis, annually impacting around 1.5 million individuals with a 40% mortality rate.[13-16] *C. albicans* virulence is intricately linked to its filamentous hyphae.[17] The hyphal morphology is associated with expression of crucial adhesins like encoded by the ALS family genes or ECE1, a gene encoding the cytolytic toxin candidalysin, both crucial for overcoming epithelial barriers and host tissue invasion.[3, 18-21] The first professional immune cells to recognize fungal pathogens are tissue-resident sentinels like macrophages, which act as essential cells to establish antifungal responses.[22-24] Although hyphal penetration of epithelial barriers is central to establish initial contact with macrophages, we know surprisingly little about their interaction with extracellular hyphae, as most of our mechanistic insight about macrophage-fungal interactions is based on infection models that start with yeast (or spore) morphologies. From those models, we have learned that filamentation, candidalysin production, and triggering of programmed cell death are key for *C. albicans* to escape clearance by this macrophage-mediated first line defense.[25-29] Filamentation here refers to intracellular germination of phagocytosed yeasts, facilitating forceful escape, which commonly causes macrophage cell death.[24, 29] Depending on the specific type of cell death, this can counterintuitively induce protective immunity. For instance,

inflammasome-driven pyroptosis leads to release of cytokines like IL-1β.[30] This promotes recruitment of further antifungal effector cells to the site of infection, particularly neutrophils, which are central for intra- or extracellular fungal clearance.[27, 31-35] By now, we know that macrophages perform limited antihyphal activities by establishing incomplete phagosomes or hyphal folding for complete internalization. [36, 37] However, it remains unclear, in how far the established concepts of macrophage killing and associated inflammatory signatures from yeast and spore interactions are transferable to the physiologically relevant scenario of immune sentinel cells initially encountering extracellular hyphae. Thus, here we studied the interaction of macrophages with extracellular fungal hyphae and demonstrate that hyphae elicit a macrophage-specific inflammatory cell death program. This process is distinct from pyroptosis, yet drives neutrophil recruitment and activation, and has implications for candidemia susceptibility.

Results

Hyphal morphology induces macrophage cell death

When encountering extracellular *C. albicans* hyphae human monocyte-derived macrophages (MDMϕ)s exhibited a substantial degree of cell death (**Figure 1A, B**). Through treatment with a fungistatic concentration of the clinical first-line antifungal caspofungin, we prevented hyphal overgrowth and compromised *C. albicans* ability to kill macrophages through nutrient depletion.[38] While this reduced total cell death induction, MDMϕs still showed similar dynamics in cell death as the infection with uninhibited hyphae for the first 15 h (**Figure 1A, B**). To fully prevent fungal nutrient consumption and active toxin production, we subsequently killed *C. albicans* hyphae with caspofungin (CKH), before exposing MDMϕs to the hyphae. Although completely inactive, CKH still elicited considerable MDMϕ death (**Figure 1C, D**). Finally, we applied heat-killing of hyphae (HKH) as a standard thorough method of microbial inactivation, which additionally denatures proteins, yet retains the hyphal morphology. Heat-inactivated hyphae still efficiently elicited cell death in MDMϕs, while yeast cells only killed macrophages when viable (**Figure 1E, F, video S1, S2**). To exclude passive candidalysin

intoxication, we used HKH of the *ece1-/-* strain, which still substantially killed MDMϕs (**Figure S2A**).[19] Importantly, HKH from different fungal species (*Aspergillus fumigatus* and *Lichtheimia corymbifera*) also significantly induced MDMϕ death **(Figure S3A, B)**. Thus, specifically hyphae, inherently retain a potential to induce cell death in primary human macrophages, even when the fungus is incapacitated in various ways.

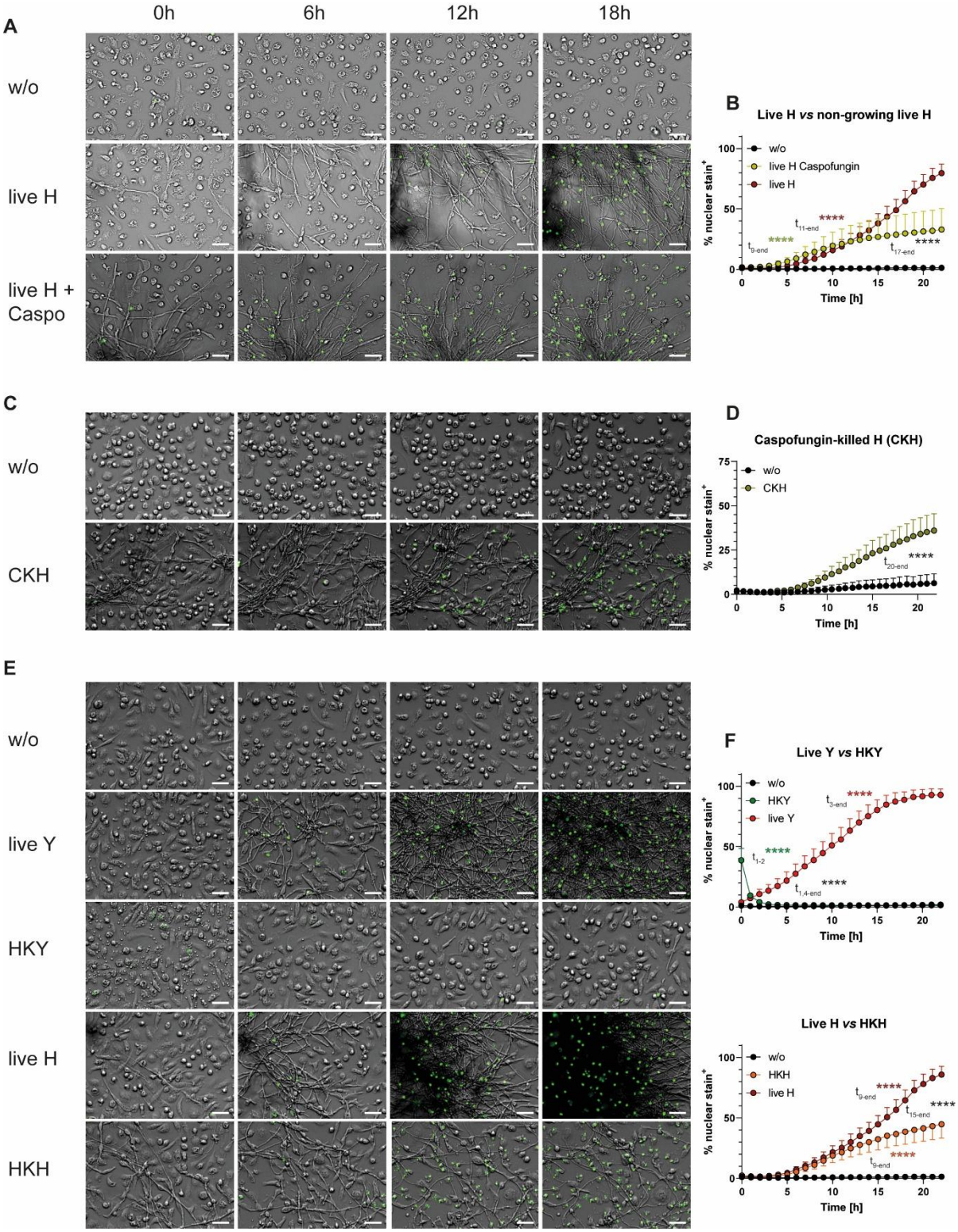


Figure 1: The hyphal morphology kills human macrophages. Live-cell imaging with SytoxGreen to visualize human MDMϕ death kinetics, triggered by different morphotypes of *C. albicans*. **(A)** Representative images and **(B)** quantification of macrophage death kinetics evaluating impact of fungal ability to grow by comparing live hyphae with live hyphae in presence of 200 ng/ml caspofungin. **(C)** Representative images and **(D)** quantification of macrophage death kinetics with caspofungin-killed hyphae. **(E)** Representative images and **(F)** quantification of macrophage death over time, comparing impact of fungal morphology and viability. MOIs: live yeasts 2.5, HKY 5, live hyphae and HKH, both 0.5; percentage cell death was calculated by normalizing SytoxGreen^{+} counts to initial total nuclei count. Scale bars represent 25 µm. Data are pooled from 6 **(A, B)**, 5 **(C, D)** or 8 **(E, F)** biologically different macrophage donors and shown as mean + SEM. Statistically significant differences were determined by Repeated-Measurements Two-Way ANOVA and Holm-Šídák post-hoc test with displayed significance symbols in the graph representing the most significant *p*-value reached in the indicated time frame of consecutive measurements "t".

Coloured symbols indicate comparisons of correspondingly coloured treatment groups against untreated, and black symbols comparisons between treatment groups. Significance levels ****$p < 0.0001$

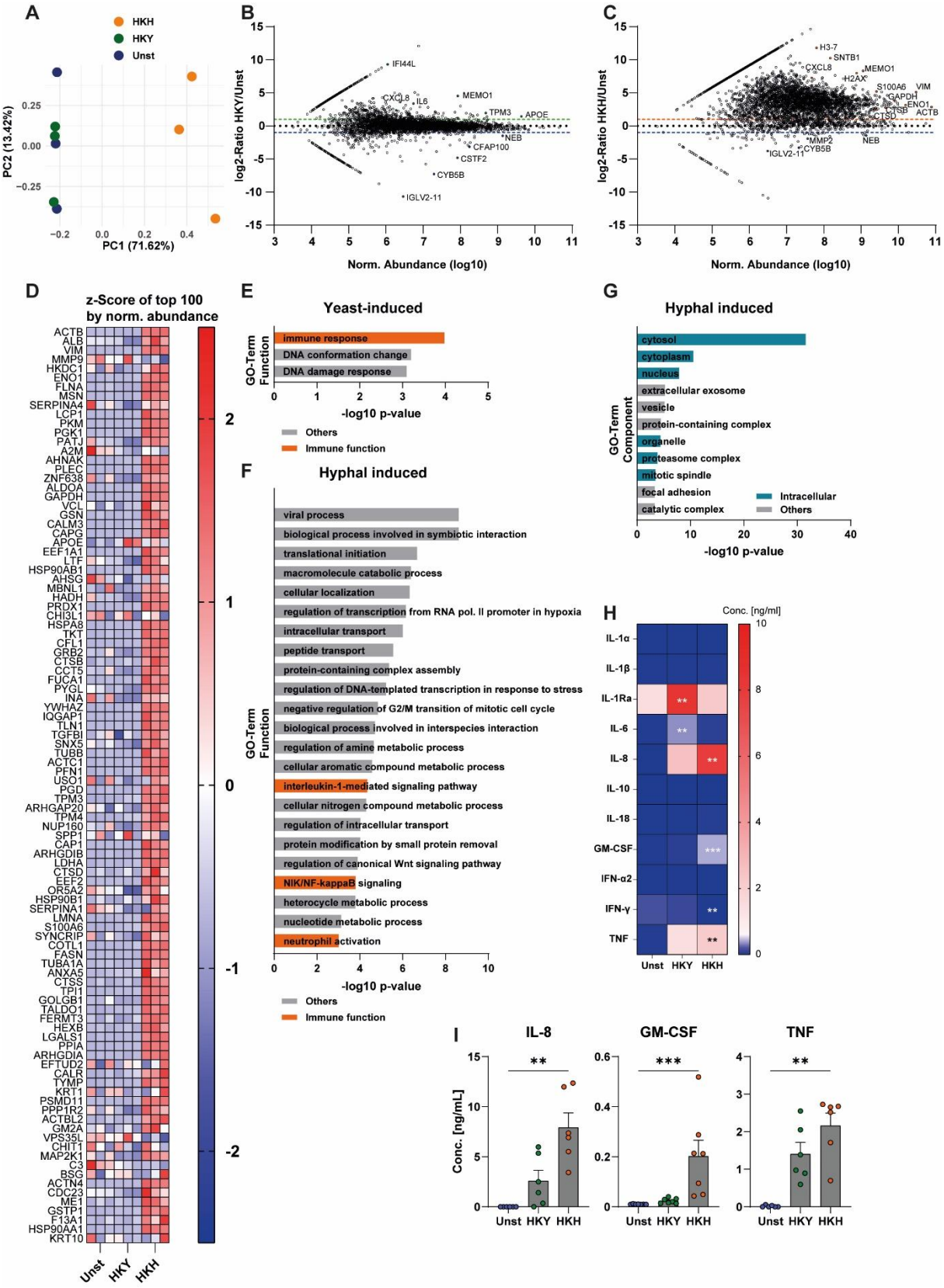
The exoproteome of hyphal interactions indicates lytic macrophage death

To delineate specific features of the hyphal morphology induced cell death, we analyzed the exoproteome of hyphal-macrophage encounters and compared it to unstimulated or yeast-stimulated macrophage exoproteomes. While yeast-stimulated MDMϕ supernatants only showed minor differences to unstimulated controls (**Ext. data 1A-C**), hyphae-stimulated exoproteomes vastly differed, showing the highest abundance and variety of proteins (**Ext. data 1A-C**). Accordingly, among the 100 top abundant proteins, most were enriched in hyphae-stimulated over yeast-stimulated or unstimulated exoproteomes (**Ext. data 1D**). Molecular Function Gene Ontology (GO) enrichment revealed functional patterns of the released proteins (**Ext. data 1E, F**). Enriched terms were "immune response" for yeast against unstimulated MDMϕ supernatants and interleukin (IL-)1 and NF-kB related signaling, as well as "neutrophil activation" for hyphal against unstimulated MDMϕ exoproteomes (**Ext. data 1E, F**). While yeast against unstimulated MDMϕ supernatants did not reveal any pattern on GO terms for Cellular Components, we found an enrichment of intracellular cytosol and nucleus-associated protein localization in hyphal against unstimulated MDMϕ exoproteomes (**Ext. data 1G**). The extracellular localization of proteins associated with central metabolism (ENO1, PGK1, PKM, ALDOA, GAPDH, LDHA), cytoskeleton (ACTB, VIM, FLNA, TUBB, TPMs), lysosomes (CTSB, CTSD, CTSS) and even nuclear proteins (LMNA), suggests an extensive lytic release of intracellular content. To estimate the immunogenicity of the supernatants, we quantified a selection of cytokines relevant to fungal infections (**Ext. data 1H**). Those already revealed a morphology-specific cytokine pattern with IL-1Ra and IL-6 preferentially in yeast-activated macrophage supernatants, while hyphae-activated macrophages released primarily IL-8, GM-CSF and TNF (**Ext. data 1H, I**). We observed similar trends by proteomics, which can, however, provide only limited information on cytokines requiring proteolytic processing to gain bioactivity (IL-1β and IL-18).[39] While proteomics suggested the presence of these cytokines, we did not measure high concentrations using ELISAs that preferentially detect the bioactive

cleaved forms. Collectively, hyphal, but not yeast-stimulated MDMϕs undergo lytic cell death and thus release intracellular proteins and inflammatory mediators into their environment.

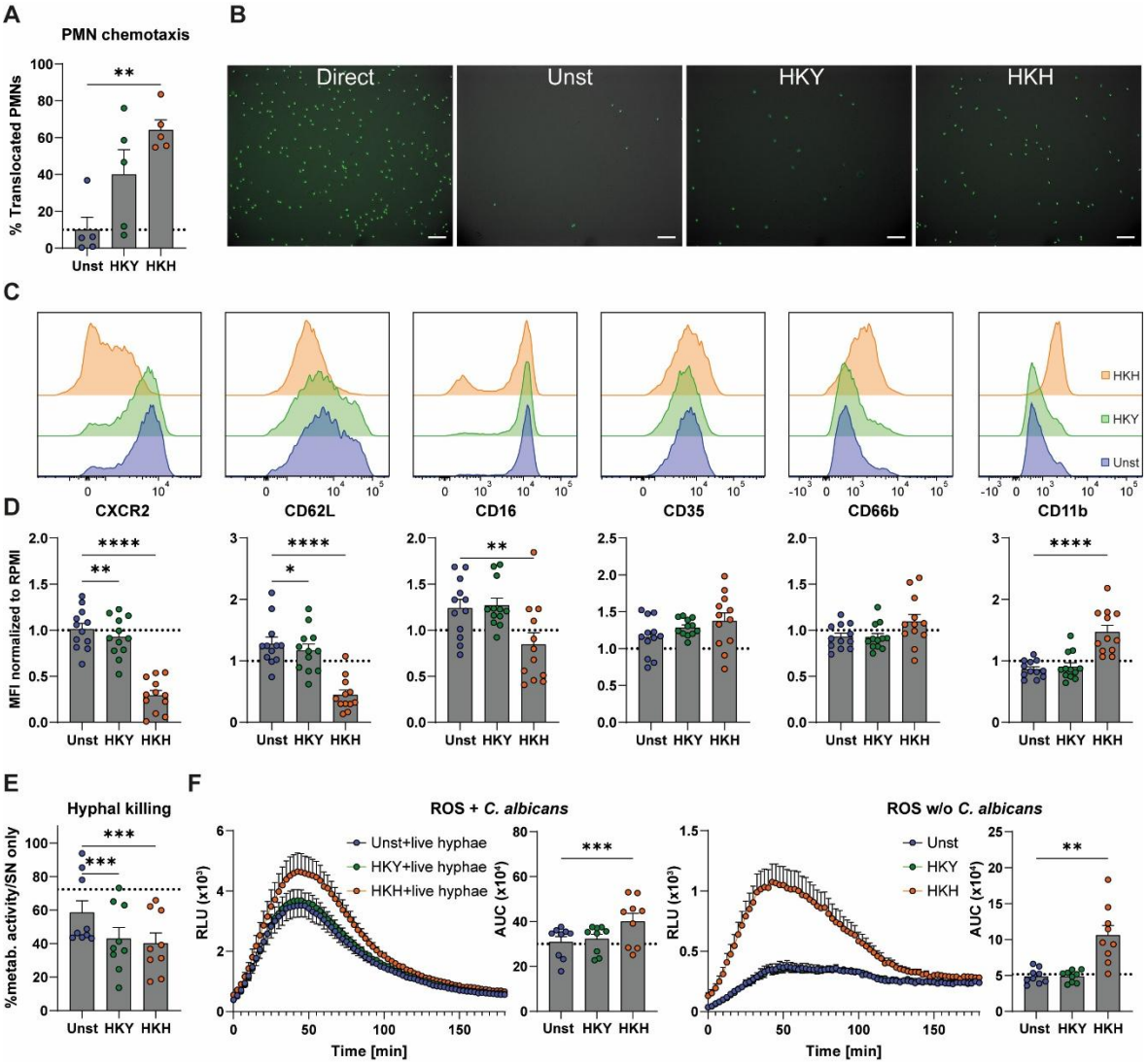
Macrophages direct neutrophil effector functions dependent on fungal morphology

As hyphal-triggered cell death was associated with the presence of well-documented neutrophil activators, we comparatively assessed downstream neutrophil recruitment and activation.[40-43] To ensure that stimulating signals were macrophage-derived, we made use of heat-inactivated *C. albicans* morphotypes. Supernatants of hyphae encounters, but not unstimulated macrophages, strongly recruited neutrophils through transwells lined with endothelial cells, while HKY-activated MDMϕ supernatants induced variable and weaker chemotaxis (**Ext. data 2D, E**). We primed human neutrophils with MDMϕ supernatants and quantified their activation by measuring surface expression of activation markers (**Ext. data 2A, B**). Specifically, macrophage supernatants from hyphae encounters potently activated neutrophils, reflected in downregulation of CD16, CD62L and CXCR2, and upregulation of CD11b. Contrastingly, supernatants from macrophage-yeast encounters, only showed small effects on activation marker regulation. Both supernatants of yeast- and hyphae-macrophage encounters primed neutrophils to kill *C. albicans* hyphae more efficiently, with the hyphal stimulation slightly more effective (**Ext. data 2C**). As key antimicrobial neutrophil effector function, we assessed reactive oxygen species (ROS) production. Priming with HKH-MDMϕ supernatants significantly increased ROS production against live *C. albicans* hyphae and it was the only supernatant that even in fungal absence significantly induced neutrophil ROS production (**Ext. data 2F**). Thus, particularly hyphal-triggered macrophage death releases inflammatory mediators that potently attract and activate neutrophils.



Extended data 1: Macrophage exoproteomes reveal morphology-specific signature of fungal stimulus. (A) PCA analysis on macrophage exoproteome according to stimulations. MA-plots of human macrophage exoproteome showing normalized abundance *vs* log2-ratio of **(B)** HKY or **(C)** HKH against unstimulated supernatants. **(D)** Z-Score over all biological replicates and conditions showing the top 100 abundant proteins (defined by mean abundance over all replicates/ conditions), ordered by abundance starting with highest. **(E-G)** GO term enrichment analysis of exoproteome with GOrilla and reduced by ReViGO,[44, 45] assessed for function of **(E)** HKY or **(F)** HKH vs unstimulated or for **(G)** cellular localization ("component") of HKH

vs unstimulated exoproteomes. Proteome data is assembled from 3 biologically different macrophage donors, their means shown in **(B, C)**. **(H, I)** Validation of proteomic data by ELISA. **(H)** Summarizing heatmap and **(I)** selected cytokines of this panel showing the HKH-induced cytokine signature. ELISA data shown as mean of 6-7 biologically different macrophage donors **(I)** with SEM and single dots for biological replicates. Statistically significant differences were determined by One-way ANOVA against the unstimulated control with Holm-Šídák post-hoc test. Significance levels $^{**}p < 0.01$, $^{***}p < 0.001$.



Extended data 2: Fungal morphology of the initial macrophage encounter determines downstream neutrophil response against *Candida albicans*. (A) Quantification and **(B)** representative images of human neutrophil chemotaxis through HUVEC-seeded transwells with MDMϕ supernatants in bottom compartment, measured after 2 h. Neutrophils were labelled with Cytopainter Green, quantified with Fiji and normalized to counts of wells, where neutrophils were added to bottom compartment directly. Single dots show combinations of 3 biologically different macrophage and 4 neutrophil donors. Scale bar represents 100 µm. **(C)** Representative histograms and **(D)** mean fluorescence intensities (MFI)s of flow cytometry for surface activation markers on human neutrophils after exposure to supernatants of MDMϕs stimulated with *C. albicans* heat-killed yeasts (HKY) or hyphae (HKH). MFI values were normalized to the same donor's RPMI control. Single dots show combinations of 4 biologically different macrophage and 3 neutrophil donors. **(E)** XTT-based assay of human neutrophil antifungal activity. Metabolic activity of 4×10^4 6 h grown SC5314 hyphae after 3 h exposure to 10^5 neutrophils, which had been preincubated for 90 min in MDMϕ supernatant (MOI 0.4). Data were normalized to the metabolic activity of the fungus in the corresponding supernatant without the presence of neutrophils. Single dots show combinations of 3 biologically different MDMϕ and 3 neutrophil donors. **(F)** Kinetic luminescence measurements and quantification of corresponding area under the curve for ROS quantification from 2×10^5 neutrophils that were stimulated with MDMϕ supernatants with or without 5×10^4 6 h grown SC5314 hyphae (MOI 0.25). Curves and single dots show combinations of 3 biologically different macrophage and 3 neutrophil donors. Bar-graphed and XY-graphed data are shown as mean + SEM with single biological replicates as dots over bars. Broken lines show mean RPMI condition as a reference. Statistically significant differences were

determined by One-way ANOVA against the unstimulated control group with Holm-Šídák post-hoc test. Significance levels *p < 0.05, **p < 0.01, ***p < 0.001, ****p < 0.0001.

C. albicans *hyphae drive rapid macrophage replacement and neutrophilia* in vivo

To define the role of this hyphal-triggered inflammatory cell death in a pathophysiological context, we adapted a *C. albicans* peritonitis model by injecting HKY and HKH intraperitoneally (*i.p.*) into immunocompetent mice. We chose this model, as the peritoneal cavity represents a relevant niche for intestinal-derived invasive *C. albicans* infections and is naturally macrophage-rich. While no significant differences for the total amount of macrophages ($CD11b^+$ / $F4/80^+$) were obvious after 24h, their composition drastically changed (**Figure 2A-D**). Hyphal injection almost completely depleted large resident TIM-4^+ macrophages and simultaneously accumulated a major population of $CD11b^+$ / $F4/80^+$ cells still carrying Ly6C, an inflammatory monocyte marker, rapidly lost after differentiation into macrophages.[46] That almost all macrophages specifically in mice injected with hyphae were TIM-4^- and $Ly6C^+$ (**Figure 2A, S1E**), indicates hyphal driven, almost complete replacement of the resident macrophage population. Paralleling the neutrophil-activating properties of human macrophage-hyphal encounters (**Ext. data 2A-F**), we observed massive neutrophilia (>5×10^6 neutrophils) in the peritoneum of hyphal-injected mice (**Figure 2E, F**). Those mice generally harbored the strongest inflammatory peritoneal cell infiltrate (**Figure 2G**). To estimate pathophysiological consequences of this process, we assessed systemic inflammation and disease severity. Hyphal-injected mice showed significantly reduced bodyweight and temperature (**Figure 2H, I**). Congruently to the human MDMϕ cytokine signature, mouse serum contained almost no IL-1β, but hyphal injection specifically induced systemic TNF responses (**Figure 2J**). Further, hyphal treatment significantly reduced circulating leukocytes, which was largely due to reduced lymphocytes, with monocytes and eosinophils following this tendency, while neutrophil counts remained stable (**Figure 2K, S3A)**. Altogether, injection of hyphae rapidly replaced resident with recruited macrophages, elicited strong neutrophilia and, in contrast to yeast injection, caused substantial systemic inflammation.

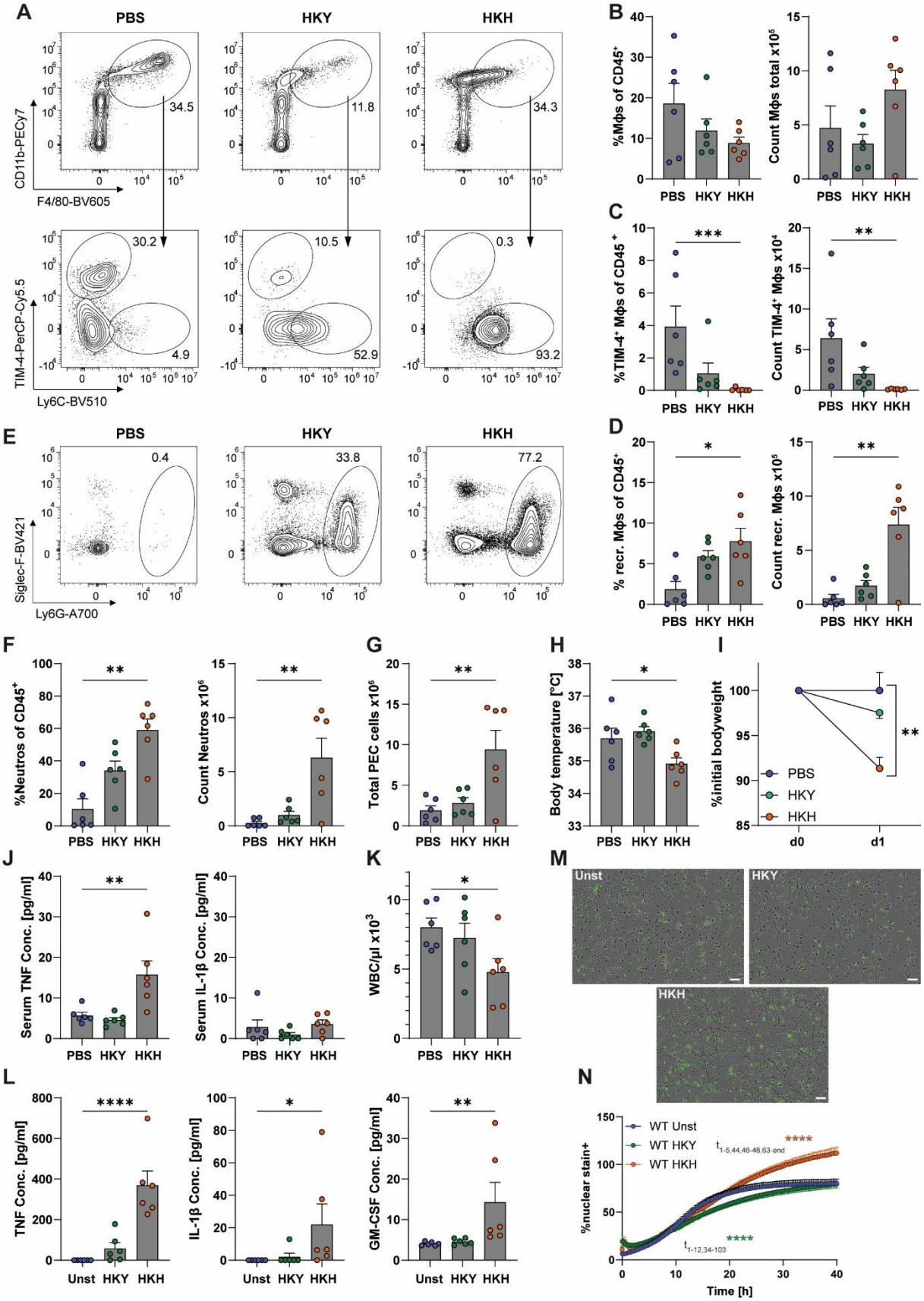


Figure 2: The hyphal morphology leads to rapid inflammatory replacement of resident peritoneal macrophages *in vivo*. Mice were treated *i.p.* with heat-killed morphologies (2×10^7 HKY or 2×10^6 HKH) of *C. albicans* and analysed after 24 h. **(A)** Exemplary FACS plots to define total peritoneal, large resident (TIM-4$^+$/Ly6C$^-$) and newly recruited (TIM-4$^-$/Ly6C$^+$) macrophages. **(B)** Percentage from CD45$^+$ and absolute numbers of total (CD11b$^+$ / F4/80$^+$) peritoneal macrophages, **(C)** large resident macrophages and **(D)** newly recruited macrophages. **(E)** Exemplary FACS plots to define peritoneal neutrophils (Ly6G$^+$) with corresponding **(F)** percentage and absolute numbers. **(G)** Total peritoneal cell infiltrate count.

(H) Facial body temperature measurement of mice. **(I)** Relative body weight loss over 24 h normalized to individual starting weight of individual mouse. **(J)** ELISA measurements for indicated cytokines from serum of *i.p.* injected mice. **(K)** Mouse white blood cell count measured by hematological analyser. **(L-N)** Peritoneal cells from untreated mice exposed to HKY and HKH *ex vivo*. **(L)** ELISA for indicated cytokines in supernatant of *ex vivo* stimulation with HKY and HKH, 40 h after stimulation. **(M)** Representative images at 36 h and **(N)** kinetic cell death quantification (SytoxGreen^{+}) of peritoneal cells, assessed by live-cell imaging. Data shown as mean + SEM and biological replicates as single dots in bar graphs. Scale bars represent 25 µm. Data are pooled from 6 mice per group. Statistically significant differences were determined by One-Way-ANOVA or Kruskal-Wallis (if non-normal distributed) or repeated measurement Two-Way ANOVA (kinetic) against untreated control group with Holm-Šídák post-hoc-testing. For *ex vivo* experiments, paired testing variants were applied. Displayed significance symbols in cell death kinetics represent most significant *p*-value reached in indicated time frame of consecutive measurements "t" with coloured symbols indicating the comparison of the correspondingly coloured treatment group against untreated. Significance levels *$p < 0.05$, **$p < 0.01$, ***$p < 0.001$, ****$p < 0.0001$.

Hyphae cause death of mouse peritoneal cells ex vivo

Macrophages have been described to disappear from the peritoneal cavity through adherence to the peritoneal wall after activation.[47] To define the nature of macrophage disappearance *in vivo*, we stimulated naïve mouse peritoneal cells *ex vivo* with fungal morphotypes and analyzed cell death kinetics by live-cell imaging. While HKY injection also trended to reduce resident macrophage numbers *in vivo* (**Figure 2A, C**), there was no evidence for cell death induction by HKY *ex vivo*, as yeast-stimulated cells contrarily even showed increased viability compared to unstimulated cells for most of the experiment. Interactions of peritoneal cells with HKH confirmatory exceeded the natural occurring cell death in the unstimulated cells significantly (**Figure 2M, N**). Consistent with our previous results, TNF was strongly released from peritoneal cells by hyphal stimulation specifically, while IL-1β and GM-CSF release, although significantly increased by hyphae, remained overall low (**Figure 2L**). Thus, we conclude that encounters with hyphae, but not yeasts, can very likely drive inflammatory macrophage death *in vivo*.

Hyphal-induced cell death is neither pyroptosis nor necroptosis

As hyphae trigger lytic, inflammatory cell death that does not rely on direct fungal actions, we were highly intrigued to unravel the underlying regulation within the host cells. Multiple pro- and anti-inflammatory cell death pathways have been described, of which inflammasome-driven pyroptosis is the most studied pro-inflammatory macrophage death in the context of *C. albicans* infections.[26-29, 48-51] To assess involvement of pyroptosis, we used inhibitors against the NLRP3 inflammasome (MCC950)

and the pyroptotic caspases 1,4/5/11 (VX-765) in human MDMϕs, and compared mouse WT bone-marrow derived macrophages (BMDMϕ)s with BMDMϕs deficient for *Gsdmd*, the terminal executor of pyroptosis.[52, 53] Surprisingly, none of these conditions prevented hyphal-induced macrophage death **(Figure S5A, B**). We further did not observe speck formation of the inflammasome adaptor ASC upon hyphal encounter, even when ASC-reporter BMDMϕs were prior primed with LPS (**Figure S5C**), matching the low IL-1β concentrations in hyphal stimulated MDMϕ supernatants. Similarly, inhibiting necroptosis with necrostatin-1, did not accomplish any rescue (**Figure S5A**). The broad caspase-like-protease inhibitor Z-VAD-FMK, moderately decreased cell death, suggesting a partial contribution of apoptotic caspases, although inflammatory cell lysis argues against apoptosis (**Figure S5A**). As we cannot consistently assign hyphal-induced macrophage death to a canonical cell death pathway, we assigned it the term “hyphoptosis”.

Hyphoptosis is controlled by specific antifungal PRRs, FAK, PI3K and ROS

To understand the pathway leading to hyphoptosis, we blocked several pattern recognition receptors (PRRs) known to recognize fungi.[54-58] Interfering with the C-type lectin receptors (CLRs) Dectin-1 and Mincle increased survival of the macrophages, with a more pronounced effect for Mincle, while Dectin-1 only modestly and late contributed to hyphal-triggered cell death **(Figure 3A, B)**. Interference with integrin CD11b proved complex, as depending on the blocked domain, cell death responses towards hyphae shifted in opposite directions. Targeting the β-glucan recognition site (M1/70) alleviated cell death, while blocking the I-domain (2LPM19c) exacerbated it (**Figure 3A**). Connecting this to the inflammatory component of hyphoptosis, TNF release was highly dependent on Dectin-1. While anti-Mincle and M1/70 did not significantly change TNF release, 2LMP19c even significantly increased it (**Figure 3C**). Downstream signaling of CLRs is largely mediated by the SYK-CARD9 axis.[58] However, we saw no impact of SYK and only a non-significant cell death trend by absence of CARD9, while it still contributed to TNF release (**Figure S6A-C**). Dectin-1 engages an additional alternative pathway *via* Raf-1.[59] Its inhibition with GW5074 improved macrophage survival, while even minorly increasing TNF

release (**Figure S6A, D**). A major downstream kinase of integrins is FAK, while both, integrins and Mincle, have been linked to PI3K signaling.[56, 60, 61] FAK inhibition with PF-573228 almost completely ablated hyphoptosis. Pan-PI3K inhibitor Wortmannin strongly improved macrophage survival, while Duvelisib, an FDA-approved inhibitor of the mostly immune cell expressed PI3K-γδ variants[62], nearly completely rescued macrophage survival (**Figure 3D, E**). FAK and PI3K pathways regulate and are regulated by ROS, which itself is a major factor in determining cell survival.[63-67] Therefore, we applied ROS-scavenging N-acetyl-cysteine (NAC) and DPI, which both strongly restored macrophage survival (**Figure 3D**). FAK inhibition also abolished TNF release, while PI3K inhibition contrastingly significantly increased it. Interestingly, ROS inhibition by DPI similar to FAK inhibition suppressed TNF release (**Figure 3F**). To validate the central role of PI3K signaling in hyphoptosis, we analyzed peritoneal cells isolated from $LysM^{Cre}$ x $PTEN^{fl/fl}$ x $R26^{tdTomato}$ mice and corresponding $LysM^{Cre}$ x $PTEN^{wt/wt}$ x $R26^{tdTomato}$ control animals *ex vivo*. In these mice, all cells expressing *Lyz2* (Lysozyme M; LysM) - mostly macrophages and neutrophils - are irreversibly labeled by expression of the fluorescent protein tdTomato. Additionally, $PTEN^{fl/fl}$ cells are deficient in PTEN, a negative regulator of PI3K signaling, resulting in constant PI3K hyperactivation.[68] By comparing the loss of $Tomato^{+}$ cells after hyphal exposure, we observed significantly increased hyphoptosis in PTEN-deficient compared to PTEN-wildtype cells, genetically confirming PI3K signaling as major driver of hyphoptosis (**Figure 3G, Figure S7A, B**). Despite ROS promoting cell death, live-cell imaging of human MDMϕs showed that fluorescence of cytosolic ROS and dead nuclei was almost mutually exclusive within the same cell at later stages (**Figure 3H**). Temporal single cell tracing revealed transient cytosolic ROS accumulation that could be lost again before the cell died. Thus, we performed single cell quantification of the timeframe between loss of cytosolic ROS and the moment of cell death. Beyond reducing overall cell death, PI3K and FAK inhibitors significantly extended the time between loss of cytosolic ROS and the moment of cell death, implying a required feedback of ROS onto PI3K and FAK to execute cell death **(Figure 3I**). Collectively, hyphoptosis is triggered *via* specific antifungal surface PRRs like Mincle,

Dectin-1 and CD11b, followed by intracellular FAK, PI3K, and ROS signaling.

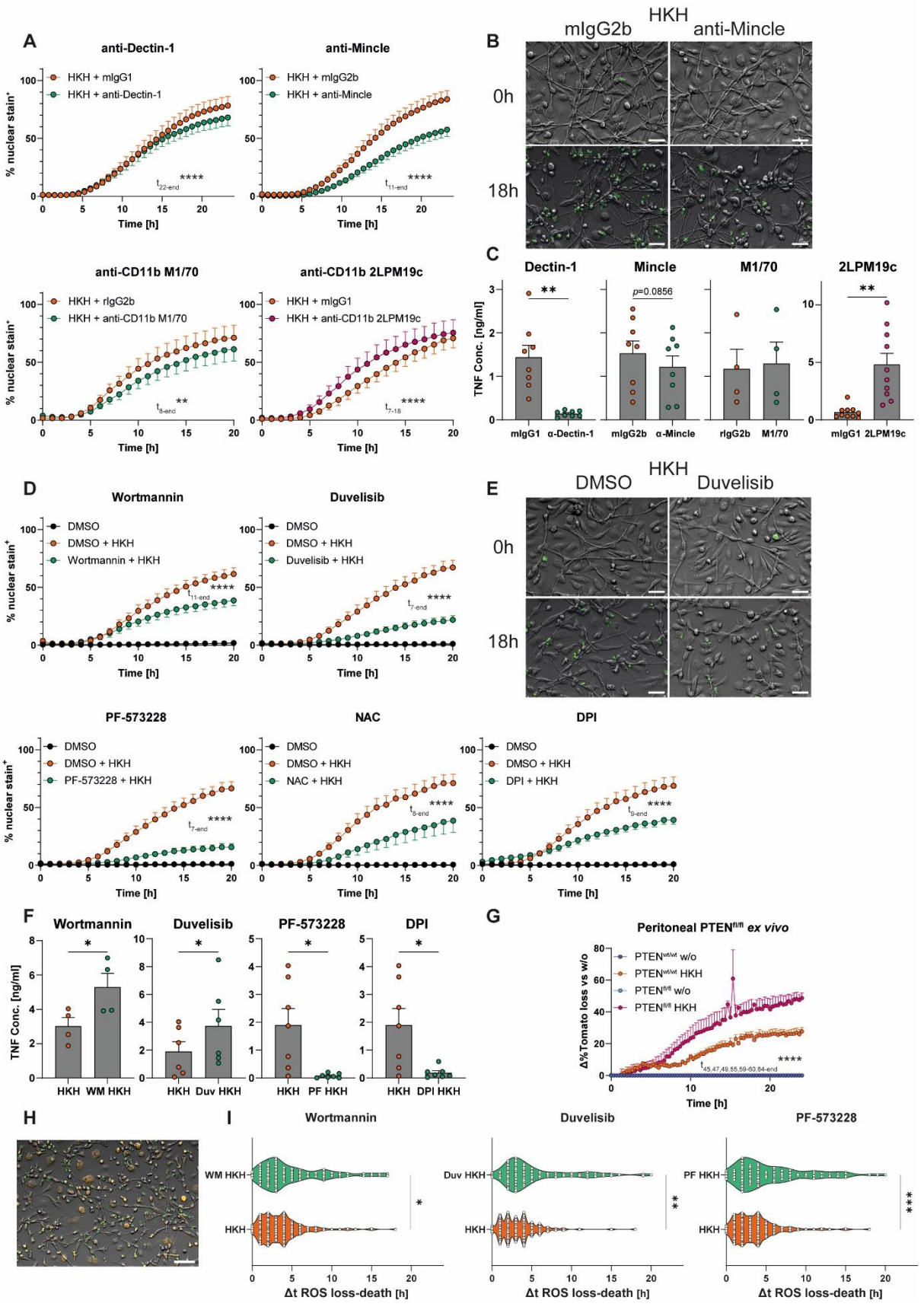


Figure 3: Hyphae-induced cell death follows engagement of antifungal receptors and downstream intracellular signaling pathways in the macrophage. Human MDMϕs were pre-treated with blocking antibodies or small molecule inhibitors

before stimulation with *C. albicans* hyphae and their cell death (SytoxGreen^{+}) was tracked over time by live-cell imaging. **(A)** Blocking of indicated antifungal surface receptors with neutralizing antibodies (10 µg/ml) and kinetic cell death quantification. Data are pooled from 8-10 biologically different macrophage donors. **(B)** Representative images of indicated timepoints from SytoxGreen live-cell imaging of MDMϕs pre-treated with anti-Mincle antibody or isotype control and stimulated with HKH. **(C)** TNF ELISA measurements from supernatants of human MDMϕs treated with blocking antibodies against antifungal surface receptors, taken 24 h post stimulation with HKH. Data are pooled from 4-10 biologically different macrophage donors. **(D)** Small molecule inhibition of signalling pathways and cell death kinetics of HKH-stimulated human MDMϕs. Inhibitor concentrations: PI3K inhibitors Wortmannin and Duvelisib 200 nM, Fak inhibitor PF-573228 10 µM, ROS inhibitors N-acetyl-cysteine (NAC) 10 µM and Diphenyleneiodonium chloride (DPI) 15 µM. Data are pooled from 11 (Wortmannin and Duvelisib), 12 (PF-573228), 4 (NAC) or 8 (DPI) biologically different macrophage donors. **(E)** Representative images of indicated timepoints from SytoxGreen live-cell imaging of MDMϕs pre-treated with Duvelisib or DMSO control and stimulated with HKH. **(F)** TNF ELISA measurements from supernatants of human MDMϕs treated with indicated small molecule inhibitors, taken 24 h post stimulation with HKH. Data are pooled from 4-8 biologically different macrophage donors. **(G)** Macrophage-specific cell death kinetics via loss of Tomato signal of PTEN-deficient (LysM^{Cre} x PTEN$^{fl/fl}$ x R26^{tdTomato}) and corresponding PTEN-wild type (LysM^{Cre} x PTEN$^{wt/wt}$ x R26^{tdTomato}) mouse peritoneal cells stimulated *ex vivo* with HKH. Data are pooled from 4-6 mice per group, normalized to their initial individual count of Tomato^{+} cells and shown as the difference between HKH and unstimulated Tomato^{+} cells of the individual animal**. (H)** Representative image of almost mutually exclusive SytoxGreen and CellRoxOrange staining 18 h after stimulation of human MDMϕs with HKH. **(I)** Single cell quantification of time difference between loss of cytosolic ROS and death (SytoxGreen^{+}) in presence of the indicated inhibitors. Where possible, 50 individual dying cells per donor of 3-4 biologically different macrophage donors in technical duplicates were temporally backtracked from their moment of death in a blinded manner. Each dot represents a single cell. Scale bars represent 25 µm **(B, E)** or 100 µm **(H)**. **(A, D)** Percentage of cell death was calculated by normalizing SytoxGreen counts to initial total nuclei count. Data are shown as mean + SEM with single biological replicates as dots for bar graphs. Statistically significant differences were determined by paired t-test or Wilcoxon if non-normal distributed (bar-graphed data) or their non-paired equivalents (violin-plotted data). Displayed significance symbols in cell death kinetics represent the most significant *p*-value reached in the indicated time frame of consecutive measurements "t", calculated by repeated measurement Two-Way ANOVA between Hyphae-stimulated groups. Significance levels *$p < 0.05$, **$p < 0.01$, ***$p < 0.001$, ****$p < 0.0001$.

Hyphoptosis is cell type-specific and restricted by physiological signals

Having identified essential signals driving hyphoptosis in human macrophages, we wondered, whether immune cells universally follow the same route. While human MDMϕs perished very vigorously and murine BMDMϕs underwent milder, but still robust hyphoptosis, primary human PBMCs contrastingly did not show any and isolated CD14^{+} monocytes only a minimal hyphoptosis phenotype (**Figure 4A**). Surprisingly, GM-CSF differentiated human MDMϕs, instead of M-CSF, were completely protected against hyphoptosis (**Figure 4B, C**). Concurrently, while M-CSF-MDMϕs constitutively accumulated cytosolic ROS over time, GM-CSF-MDMϕs did not, even when encountering fungal hyphae (**Figure 4C, D**). We did not observe a consistent difference for TNF release between M-CSF-MDMϕ and GM-CSF-MDMϕs, highlighting that GM-CSF-MDMϕs responded to the hyphae, but did not die during the encounter (**Figure 4E**). Consequently, we characterized differences in responses of M-CSF- and GM-CSF- differentiated MDMϕs to fungal hyphae by flow cytometry 90 min after stimulation (**Figure 4F, G, Figure S1C-E**). M-CSF-MDMϕs expressed significantly more β-glucan receptor Dectin-1, which was surface-downregulated upon interaction with fungal elements indicating receptor engagement and

internalization. Mincle expression appeared generally low at this time point resulting only in a mild trend of downregulation in M-CSF-MDMϕs after encountering hyphae. The mannose receptor CD206 was significantly higher expressed in GM-CSF-MDMϕs, though not changed by stimulation. Similarly, CD11b expression was higher in GM-CSF-MDMϕs and even increased in those after hyphal exposure. For interpretation, we pre-gated on CD11b and used the I-Domain binding clone ICRF44. GM-CSF-MDMϕs expressed also more HLA-DR and the integrin CD11c, two proteins broadly induced upon activation.[69-71] Both were moderately upregulated by hyphal contact in both macrophage types, though more pronounced in M-CSF-MDMϕs. GM-CSF-MDMϕs stored significantly more intracellular TNF than M-CSF-MDMϕs, while GM-CSF was higher in M-CSF-MDMϕs, yet both did not change significantly after stimulation with hyphae. Interestingly, GM-CSF-MDMϕs displayed higher baseline phosphorylation of FAK and the PI3K target AKT compared to M-CSF-MDMϕs. Contrastingly, GM-CSF-MDMϕs did not alter FAK or AKT phosphorylation levels after fungal exposure, while M-CSF-MDMϕs significantly increased AKT phosphorylation upon exposure to yeasts and hyphae, and FAK phosphorylation upon hyphal stimulation specifically. This collectively emphasized an overall stronger early responsiveness against hyphae in M-CSF-MDMϕs compared to GM-CSF-MDMϕs, especially for molecules mechanistically involved in hyphoptosis like Dectin-1, PI3K surrogate AKT and FAK (**Figure 4G**). Given the contrast between M-CSF- and GM-CSF-MDMϕs in undergoing hyphoptosis, we hypothesized that specific cytokines could program resistance into previously susceptible macrophages. Indeed, after 9 days of replacing M-CSF with GM-CSF, former M-CSF-MDMϕs had become almost fully resistant against hyphoptosis (**Figure 4H, J**). We tried a similar approach with IL-4 that we added to fully differentiated M-CSF-MDMϕs for 9 more days together with M-CSF, which enriched for multinucleated giant cells.[72] Likewise, prolonged IL-4 treatment significantly improved macrophage survival against hyphal exposure (**Figure 4I, K, Video S3**), overall demonstrating that our immune system can regulate and limit hyphoptosis, when needed.

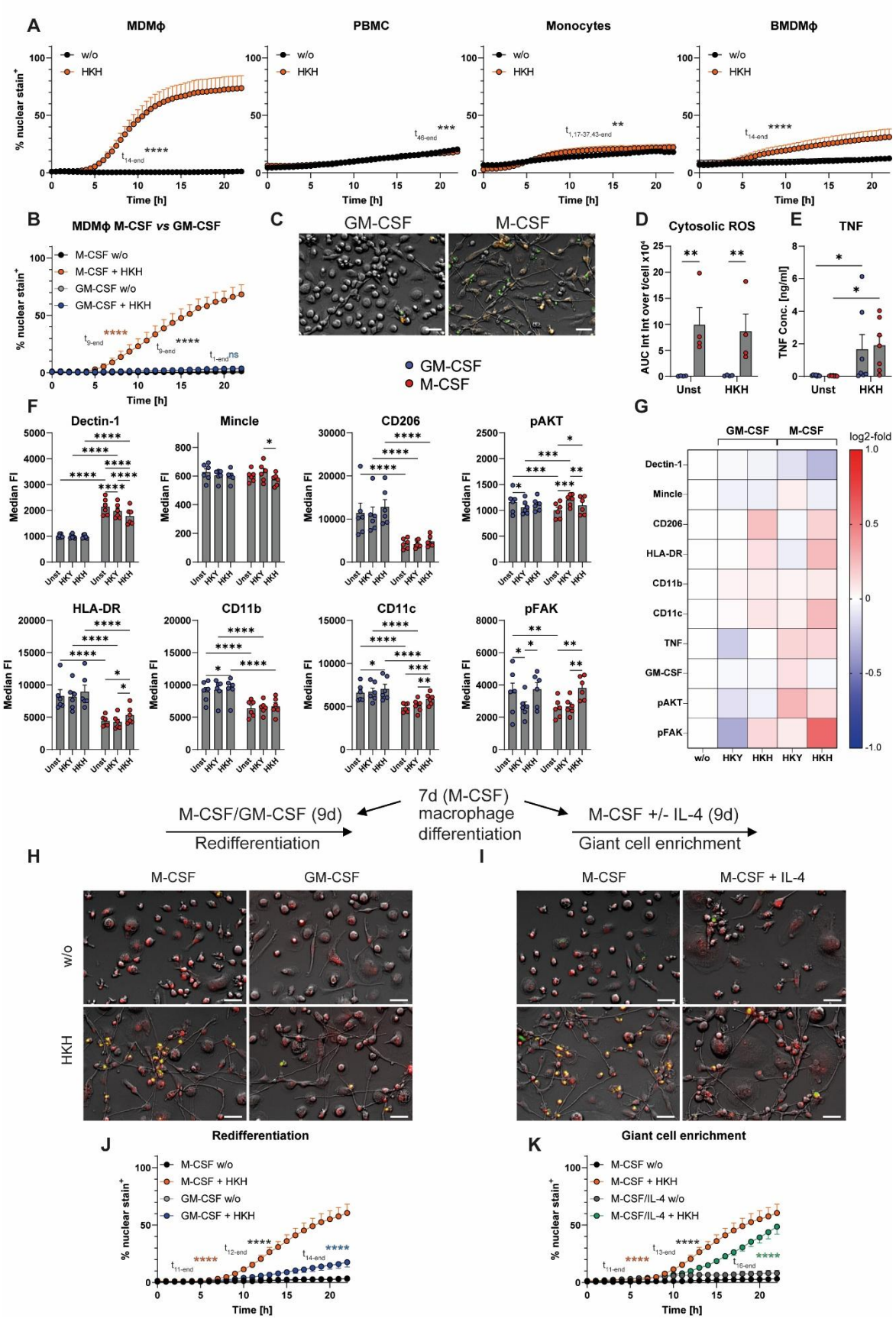


Figure 4: Hyphoptosis occurs specifically in M-CSF-dependent macrophages and can be tolerized against by prolonged treatment with GM-CSF or IL-4. (A) Cell death kinetics (SytoxGreen⁺) of HKH-stimulated or unstimulated human M-CSF-differentiated macrophages (6 donors), PBMCs (7 donors), CD14⁺ monocytes (4 donors) and mouse M-CSF-differentiated mouse BMDMϕ (7 mice). **(B)** Cell death kinetics (SytoxGreen⁺) of human GM-CSF *vs* M-CSF differentiated macrophages (8

donors, paired) with or without HKH stimulation. Data were additionally normalized by subtracting individual cell death at t_0 to correct for different starting points between M-CSF and GM-CSF. **(C)** Representative images of live cell imaging co-staining of SytoxGreen and CellRoxOrange in HKH-stimulated GM-CSF or M-CSF differentiated macrophages 18 h post stimulation. **(D)** Quantification of intracellular ROS signal of human GM-CSF *vs* M-CSF differentiated macrophages with or without HKH stimulation, quantified by area under the curve of the integrated CellRoxOrange intensity over time per initial cell number on the image of 4 biologically individual, paired donors. **(E)** TNF release by ELISA on supernatants of human GM-CSF *vs* M-CSF differentiated macrophages with or without HKH stimulation of 7 biologically individual, paired macrophage donors. **(F)** Selection of median fluorescence intensities and **(G)** heatmap overview of flow cytometry on cell death pathway/polarization/activation-associated markers on human GM-CSF *vs* M-CSF differentiated macrophages with or without HKY or HKH stimulation, 90 min post stimulation. Data are pooled from 6 biologically different, paired macrophage donors. Bar graphs show raw median fluorescence intensities, heat map shows normalized values to corresponding differentiation's unstimulated controls. Macrophages after full differentiation with M-CSF were for 9 days treated with **(H, J)** GM-CSF to redifferentiate them or **(I, K)** IL-4 to enrich for multinucleated giant cells. **(H)** Representative images at 18 h post stimulation and **(J)** cell death kinetics of M-CSF control and GM-CSF redifferentiated human macrophages stimulated with HKH. **(I)** Representative images at 18 h post stimulation and **(K)** cell death kinetics of M-CSF control and M-CSF + IL-4 treated human macrophages stimulated with HKH. Scale bars represent 25 µm. Data are pooled from 6 biologically individual, paired donors. Data presented as mean + SEM with single biological replicates as dots for bar graphs. Green shows SytoxGreen$^+$ dead nuclei, red shows SytoDeepRed$^+$ all nuclei to visualize multinucleated status of giant cells. Statistically significant differences were determined by Two-Way ANOVA with Holm-Šídák post-hoc test. For cell death curves, statistically significant differences were determined by Repeated-Measurements Two-Way ANOVA and Holm-Šídák post-hoc test with displayed significance symbols representing the most significant *p*-value reached in the indicated time frame of consecutive measurements "t". Coloured symbols indicate the comparison of correspondingly coloured treatment groups against untreated and black symbols comparisons between treatment groups. Significance levels *$p < 0.05$, **$p < 0.01$, ***$p < 0.001$, ****$p < 0.0001$.

Inhibiting hyphoptosis improves macrophage performance against viable hyphae

As viable *C. albicans* hyphae induce macrophage cell death trough several mechanisms, we had to make use of inactivated hyphae to dissect the underlying host signaling pathways of hyphoptosis. Naturally, we were intent to unravel how hyphoptosis plays a role in the interaction between macrophages and viable hyphae. Therefore, we used three of our most-promising hyphoptosis-protective treatments on human MDMϕs before infecting them with live *C. albicans* hyphae: Inhibition of FAK or PI3Kγδ or differentiation with GM-CSF. Using a live-cell imaging "dual killing" assay, we dynamically quantified macrophage death and restriction of hyphal growth. Both, inhibition of FAK and PI3Kγδ significantly improved macrophage survival against live hyphae. Hyphal growth inhibition remained similar to DMSO controls, with slight advantages for PI3Kγδ-inhibited macrophages (**Figure 5A, B**). Notably, this was specific to hyphae, as when performed with viable yeasts, FAK-inhibited macrophages quickly lost control and PI3Kγδ inhibition had no effect (**Figure S8A, B**). This, suggests that survival advantages against hyphae specifically stem from preventing hyphoptosis. Alternative differentiation with GM-CSF completely rescued macrophages and furthermore significantly improved hyphal growth inhibition compared to hyphoptosis-sensitive M-CSF-MDMϕs (**Figure 5C**). Beyond, GM-

CSF-MDMϕs acquired improved resilience against live yeasts and at later time points (after germination to hyphae), also showed significantly improved fungal growth restriction (**Figure S8C**). According to our results, hyphoptosis is mechanistically independent of candidalysin, but as this is a well-established fungal virulence factor, comparing their individual impact on macrophage cell death, might give us an approximation about the importance of hyphoptosis in a real infection.[19, 27-29, 31, 73, 74] Candidalysin deficiency (*ece1-/-*) alleviated macrophage death (**Figure 5D**) to a similar degree as inhibiting hyphoptosis with PF-573228 or Duvelisib, while hyphoptosis-protected GM-CSF-MDMϕs outperformed all other conditions. Thus, inhibiting crucial elements of the hyphoptosis pathway improves macrophage survival against viable hyphae.

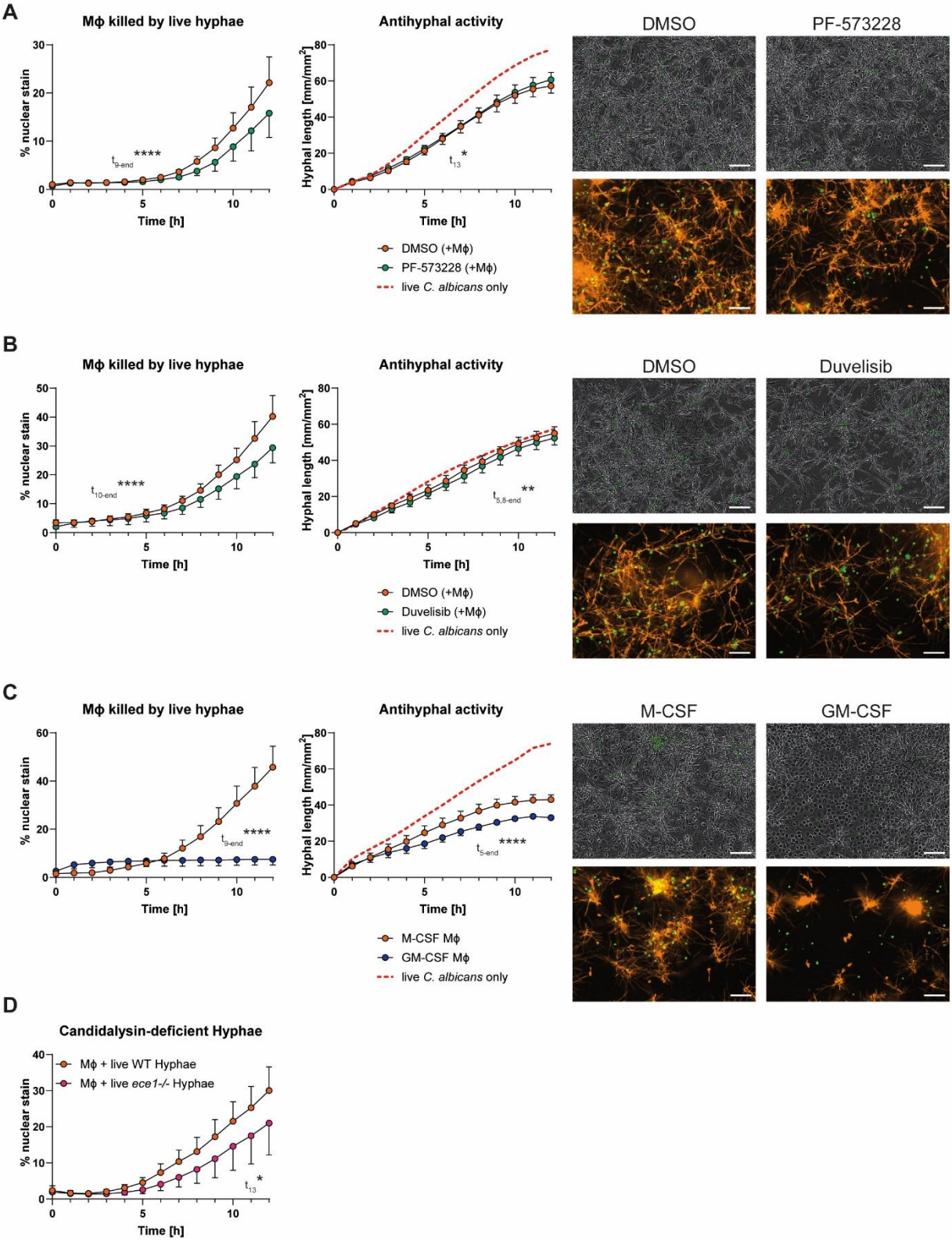
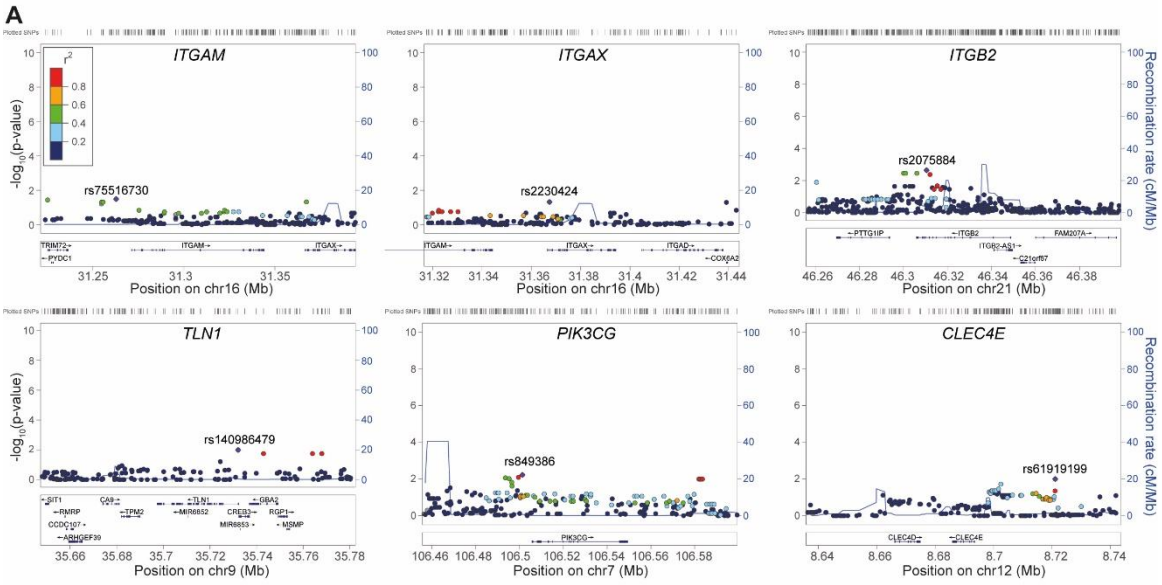


Figure 5: Inhibition of hyphoptosis improves macrophage performance against viable hyphae. hMDMϕs were confronted with viable SC5314-mScarlet hyphae (MOI 0.25) and followed by live-cell imaging. Mϕ death kinetics (SytoxGreen$^+$) and (Mϕ-)permitted hyphal outgrowth quantification over time ("dual killing assay") including representative images (10 h) of combinations of phase contrast or fungal expressed mScarlet with SytoxGreen, under hyphoptosis-inhibiting conditions via **(A)** 10 µM PF-573228 (5 donors), **(B)** 200 nM Duvelisib (4 donors), **(C)** alternative differentiation with GM-CSF (5 donors). **(D)** Mϕ death kinetics confronted with WT or *Ece1-/-* BWP17 Clp30 *C. albicans* hyphae as comparison for effect size (8 donors). Significance levels *$p < 0.05$, **$p < 0.01$, ****$p < 0.0001$.

Genetic variation in hyphoptosis-associated genes affects susceptibility to candidemia

To estimate potential consequences of dysregulated hyphoptosis induction for candidemia development, we assessed genetic variation for a few selected candidate genes, based on their mechanistic involvement in hyphoptosis (**Figure 3**), in a candidemia cohort.[75] We looked for single nucleotide polymorphisms (SNP)s in Mincle (*CLEC4E*), PI3K-γ/δ variant genes (*PIK3CG, PIK3CD*) and the integrin-signaling associated molecules CD11b (*ITGAM*), its close relative CD11c (*ITGAX*), their heterodimeric binding partner CD18 (*ITGB2*)[76], FAK (*PTK2*), FAK2 (*PTK2B*) and talin-1 (*TLN1*), a close interaction partner of FAK[77] downstream of integrins. The results of the targeted association analysis were visualized using regional association plots to highlight significant SNPs (**Figure 6A**). Within *ITGAM, ITGAX, ITGB2, TLN1, PIK3CG,* and *CLEC4E* gene regions, we identified SNPs (rs75516730, rs2230424, rs2075884, rs14098647, rs61919199, and rs849386, respectively) that were associated with patients' susceptibility to candidemia. The intronic SNP rs2075884 in *ITGB2* exhibited the strongest association (p-value = 2.3 x 10^{-3}). To functionally link these SNPs, we queried the eQTLGen phase I database[78] for their impact on gene expression. All SNPs except for the upstream gene variant rs140986479 in *TLN1* and rs75516730 in *ITGAM* were expression Quantative Trait Loci (eQTL) associated with altered expression levels of their corresponding target genes in whole blood (**Figure 6B**). Interestingly, the *ITGAM* SNP rs75516730, similar to rs2230424 in *ITGAX* itself, influenced the expression of *ITGAX*, with the latter one additionally influencing *ITGAD* expression. SNP rs61919199 in *CLEC4E* does not only alter gene expression of *CLEC4E*, but affects also expression of other Dectin-2 family members, though weaker and in opposite direction. A detailed summary of the top SNPs and their impact on directional gene expression is presented in **Figure 6B**. Exemplary, rs2075884 in *ITGB2* (p-value = 0.002) with an estimated odds ratio of 0.55 links a lower chance of candidemia to carriers of the minor allele, which is also associated with a significantly lower expression of *ITGB2* in whole blood. Apart from rs849386 in *PIK3CG*, for all variants that directly influenced gene expression of their own or a closely related gene, higher expression correlated with elevated risk of candidemia. Overall, this observation suggests

that genetic variants in hyphoptosis-associated genes may influence expression levels of nearby genes to contribute to candidemia susceptibility.



B

OR
2
1.5
1
0.75
0.5

z-score
20.0
10.0
0
-10.0
-20.0

Candidemia association						eQTL		
SNP	Gene	Minor allele	OR	*p*-value	Risk allele	Affected gene	z-score	*p*-value
rs75516730	***ITGAM***	T	**1.82**	0.032	T	*ITGAM*	**n/a**	n/a
						ITGAX	**12.3**	1.48E-34
rs2230424	***ITGAX***	C	**1.62**	0.048	C	*ITGAX*	**13.6**	2.84E-42
						ITGAD	**8.1**	7.99E-16
rs2075884	***ITGB2***	T	**0.55**	0.002	C	*ITGB2*	**-11.6**	4.18E-31
rs140986479	***TLN1***	C	**0.39**	0.010	T	*TLN1*	**n/a**	n/a
						GBA2	**-10.7**	1.14E-26
						TPM2	**18.3**	1.48E-74
rs849386	***PIK3CG***	A	**1.72**	0.006	A	*PIK3CG*	**-11.4**	2.61E-30
rs61919199	***CLEC4E***	T	**0.63**	0.010	G	*CLEC4E*	**-16.5**	2.77E-61
						CLEC6A	**5.2**	1.71E-07
						CLEC4D	**10.9**	1.07E-27

Figure 6: Candidemia patients display genetic variation in many selected genes associated with the hyphoptosis pathway. **(A)** Regional association plots highlighting the top SNPs in candidate gene regions. The -log10 *p*-values of SNPs are plotted on the y-axis against their physical position (NCBI build 36) on the x-axis. The most strongly associated SNPs in the regions are represented with purple diamond and surrounding markers are colour coded according to their correlation coefficient (r^2) with the top SNP using the hg19/1000 Genomes European samples. Light blue lines denote estimated recombination rates. Association *p*-values of the top SNPs in various gene regions are overlaid on the plots. **(B)** A table representing the summary statistics of the significant top SNPs in each gene region combined with variant-specific gene expression data in whole blood derived from the eQTLGen phase I database.[78] Abbreviations: SNP (single nucleotide polymorphism)s; OR (estimated odds ratio). An OR above 1 indicates that the minor allele is more frequent in candidemia patients than in healthy controls and therefore the risk allele. Z-scores above 0 indicate a positive association of the minor allele with gene expression levels of the affected gene in whole blood.

Discussion

Here we reveal a previously overlooked, macrophage-specific, inflammatory cell death pathway ("hyphoptosis"), that is triggered by hyphae across different fungal pathogens and is associated with implications for genetic susceptibility to candidemia. Hyphoptosis is a host-driven cell death response to fungal hyphae, that does not essentially require their viability. Hyphoptosis is strongly induced in

M-CSF differentiated human macrophages *in vitro*, but occurred also in mouse bone marrow-derived and peritoneal macrophages. Both *in vitro* and *in vivo*, hyphoptosis was revealed to be a strong driver of neutrophilic inflammation. We characterized crucial players in the hyphoptosis cell death pathway, which clearly distinguish it from pyroptosis. Inhibiting essential players in its pathway improves macrophage survival when interacting with viable hyphae, consequently we consider hyphoptosis as another mechanistic layer of macrophage cell biology in response to filamentous fungi. Finally, by repurposing small molecule inhibitors and recombinant cytokines, we provide potential immunotherapeutic possibilities to target hyphoptosis. Our study highlights that the initial encounter of fungi with macrophages dictates downstream immune activation in a morphology-dependent way, although the recruited effector cell has never seen the corresponding morphology. Supported by the observation of a rapid macrophage replacement *in vivo*, it is plausible to assume that hyphoptosis occurs early during infection, when sentinel macrophages encounter first hyphae that pierce through barrier tissue. Further, the hyphoptosis-derived proinflammatory lytic proteome coupled with neutrophil activation across several read-outs, propose it as an immunological communication to relay the signal of a "larger pathogen" to early recruited immune cells. Collectively, the combined increase in neutrophil chemotaxis and oxidative responses could translate to enhanced swarming, an efficient mechanism against clusters of hyphae.[33] How immune cells distinguish fungal morphologies and communicate this to other immune cells has been a recurrent topic with most literature arguing with differences in cell wall composition, pathogen size and intra-or extracellular ROS accumulation.[34, 35, 79-83] Likely all these aspects are important for the cellular decision, whether to undergo hyphoptosis, which in turn contributes to accordingly shape the direction of the immune response. Whether this process is per definition beneficial, is questioned by the genetic associations we identified, where an overexpression of several pathway participants correlates with a higher risk to develop candidemia. This suggests a context-dependent function that needs tight regulation as it harbors the danger of both immunosuppression by eradicating macrophage-mediated defense and immunopathology by excessive neutrophil recruitment and activation. As the minimum requirement to engage the pathway

are dead fungal filaments, hyphoptosis might have therapeutic implications by maintaining inflammatory immunopathology in patients, even when the pathogen is successfully controlled by antifungals. This idea is supported by our *in vivo* results, where dead fungal hyphae still caused drastic systemic inflammation including a weight loss of almost 10% within one day, raising parallels to a scenario of LPS causing septic shock in patients, even though the bacterial infection has been cleared with antibiotics.[84] Generally, our mouse *i.p.* model replicated central observations with primary human macrophages *in vitro*: rapid macrophage depletion, strong TNF release and neutrophilic inflammation. That hyphae triggered inflammatory cell death in peritoneal cells *ex vivo* further substantiates that hyphoptosis and the associated neutrophil activation occur *in vivo.* Mechanistically, we identified the CLRs Dectin-1 and Mincle, as well as the integrin CD11b as drivers of hyphoptosis. Further integrins are likely to participate, but none of them are as well characterized as CD11b in the context of fungal infections, which unfortunately limits binding-site-specific tools for other integrins. Interestingly, the CD11b-β-glucan recognition domain and I-domain seem to have opposing functions in the regulation of hyphoptosis. In this context, the I-domain has recently been suggested to bind ALS proteins of *C. albicans*, hinting at a differential hyphoptosis regulation defined by binding of CD11b to different ligands on the fungal surface. The ALS-CD11b interaction downstream was shown to activate the NLRP3 inflammasome.[85] At first unexpectedly, we encountered several lines of evidence that the observed hyphal-triggered cell death cannot be called canonical (NLRP3-) inflammasome-driven pyroptosis, nor does it fit well with the canonical cell death pathways necroptosis and apoptosis, as it cannot be inhibited with necrostatin and is anything but “silent”, respectively. The β-glucan-Dectin-1-SYK-CARD9 axis represents the major driver of the accompanying inflammatory cytokine release, for the actual cell death execution its role is limited. Rather FAK downstream of integrins, centrally orchestrated both inflammation and cell death. Counterintuitively, we identified the PI3K-pathway, a pathway commonly associated with survival and proliferation, central for hyphal-triggered cell death.[86] The PI3K-γ/δ-specific inhibitor Duvelisib prevented death more potently compared to pan-PI3K inhibitor Wortmannin, not excluding that PI3Kα/β might actually transmit pro-survival signals. Both,

integrins and Mincle have been associated with PI3K signaling in fungal infections, with the latter receptor even described to context-dependently counteract Dectin-1/2 mediated immunity.[56, 87, 88] Accordingly, while preventing cell death, PI3K inhibition elevated inflammatory cytokine release, which further confirms the model that it acts downstream of FAK.[89] Importantly, peritoneal macrophages deficient for the PI3K antagonist PTEN perished faster, genetically reaffirming PI3K's central role to execute hyphoptosis.

We established tolerance to hyphoptosis by either differentiating macrophages with GM-CSF, or adding GM-CSF or IL-4 to fully M-CSF-differentiated macrophages for a prolonged time. The tolerance induction parallels the trained immunity concept, which has been described for both cytokines in different contexts.[90, 91] Seemingly contradictory to this, inhibiting PI3K, which is essential to establish trained immunity has an immediate effect to prevent hyphoptosis, even more confusingly so, as both GM-CSF and IL-4 are potent inducers of PI3K signaling.[92-94] Considering the different kinetics of the described effects, we conclude that previous non-lethal PI3K activation primes a cellular state of higher tolerance against later lethal PI3K overactivation, presumably by so far unknown feedback-loops. A similar concept has been postulated in cancer cells, where in line with our observations, hyperactive PI3K-AKT signaling does not necessarily ensure proliferation and tumor cell survival, but can potentially lead to ROS-mediated cell death.[67, 95] In line with this an interesting hypothesis is raised on cancer cell adaptation to higher levels of PI3K signaling in genetic absence of PI3K antagonist SHP-1, possibly resembling a "trained phenotype".[67] The basis for this phenomenon alludes to regulation of cellular metabolism, an avenue, warranting future exploration for hyphoptosis.

The genetic associations of hyphoptosis-associated genes in candidemia patients might be attributed to further roles in immunity beyond hyphoptosis.[54, 55, 96-98] Nonetheless, our findings likely translate to other fungal diseases, as hyphae of different human fungal pathogens can trigger hyphoptosis. Accordingly, we previously discovered the pyroptosis/necroptosis-independent depletion of alveolar macrophages by *Aspergillus fumigatus* in a mouse airway allergy model.[99] This depletion involved cell death, repolarization and giant cell formation, strongly promoted by IL-4, thereby unifying aspects of

hyphoptosis and adaptive training into hyphoptosis resilient cells.[99] Training patient cells for elevated antifungal immunity appears increasingly attractive as adjunctive immunotherapy.[100-103] Hyphoptosis and its stimulatory effects on recruited effector cells could represent a promising target for personalized immune modulation in severe fungal infections. In patients with defects in immune cell functionality, pathogen recognition or downstream signaling, artificially engaging the pathway might have adjuvant-like properties to compensate otherwise lacking immune activation. Contrastingly, in neutropenic patients, hyphoptosis inhibition might be desirable to maintain macrophage-mediated defense. In this case, adjunct therapy with an anti-leukemia-repurposed PI3K-γ/δ inhibitor like Duvelisib that inhibits hyphoptosis but not macrophage activation could be considered. Alternatively, "training" with recombinant GM-CSF that tolerizes against hyphoptosis, improves antifungal activity and additionally promotes granulocyte mobilization, might prove promising to further pursue.[104] Overall, we provide mechanistic insight into an unconventional inflammatory, macrophage-specific cell death triggered by fungal hyphae. We demonstrate, genetic variation in this pathway occurs with altered frequency in candidemia patients, and explore immunotherapeutic angles to potentially modulate the "hyphoptosis" pathway in future patient care.

Online Methods

Study approval

Experiments involving human blood were conducted in accordance with good clinical practice, the Declaration of Helsinki and approved by the ethics committee of Jena University Hospital (Permission No 2207-01/08). Only after obtaining written informed consent, healthy individuals were included as blood donors.

Human immune cell isolation and differentiation

Human peripheral blood mononuclear cells (PBMC)s were isolated from buffycoats or freshly drawn venous blood by density gradient centrifugation over Lymphocyte Separation Medium (Capricorn), Density 1.077 g/ml in 50 ml sterile tubes. Neutrophils were isolated from the erythrocyte/granulocyte

fraction by hypotonic lysis of the erythrocytes in 155 mM NH_4Cl, 10 mM $KHCO_3$. Afterwards, neutrophils were washed twice in PBS and resuspended in RPMI-1640 including 2 mM L-glutamine (RPMI, Gibco). $CD14^+$ monocytes were isolated from the PBMC interphase with magnetic beads and automated cell sorting (autoMACS; MiltenyiBiotec). PBMCs, neutrophils and monocytes were seeded in 96-well plates and used for experiments directly. To differentiate human monocyte-derived macrophages (MDMϕ)s, 10^7 monocytes were seeded into 175 cm^2 cell culture flasks (Sarstedt) in RPMI including 10% heat-inactivated fetal bovine serum (Bio&Sell) and 50 ng/ml recombinant human macrophage-colony-stimulating factor (M-CSF) or granulocyte-macrophage-stimulating factor (GM-CSF) (both Immunotools) for 7 days with a full medium exchange on day 5. Macrophages were detached from cell culture flasks by 20 min exposure to 10 mM EDTA and gentle cell scraping on day 7. $4x10^4$ MDMϕs were seeded per well into 96-well plates. For re-differentiation of M-CSF-MDMϕs into GM-CSF-MDMϕs in 96-well plates, cells were switched from M-CSF to 50 ng/ml GM-CSF on day 8 and cultured like this for 9 days with half-exchange of medium on days 9 and 14 and a full medium exchange on day 12. For enrichment of multinucleated giant cells, MDMϕs were treated accordingly, but instead switched to 50 ng/ml M-CSF plus 50 ng/ml IL-4 (Immunotools).

Fungal culture and stimuli preparation

Candida albicans strain SC5314 (ATCC MYA-2876) was used in all experiments. It was kept on YPD agar plates for up to 4 weeks, before starting a new culture from cryostocks. The afternoon before the experiment, a single colony was inoculated into liquid YPD culture for a fresh overnight culture. This was washed 3x in PBS, before further use. For generating killed fungal stimuli, the washed overnight yeast culture was either directly heat-killed (HKY) in a heating block at 90 °C for 60 min or cultured shaking for up to 16 h in RPMI, pH 6.4 at $4x10^5$/ml to generate a low-aggregated hyphal culture. This was washed twice in PBS and also heat-inactivated under the same conditions (HKH). After heat-killing, fungal stimuli were washed again in PBS twice, and hyphae were concentrated to 10^7/ml according to their yeast count at the start of the culture before storage at -20 °C. Other fungal species

Aspergillus fumigatus (ATCC 46645) and *Lichtheimia corymbifera* (CBS 429.75) were grown on potato dextrose agar, but after spore harvest, HKH were analogously generated. For caspofungin-killing, after 16 h culture in RPMI, hyphae were switched to PBS and exposed to 50 µg/ml Caspofungin (Sigma-Aldrich) for 24 h shaking at 37 °C (CKH). Complete killing was confirmed by plating on YPD agar.

Mice and infection model

Card9-/-[105], *Gsdmd-/-*[53], conditional LysM-specific *Pten* knockout mice harboring a Rosa26-tdTomato fate-mapping construct ($LysM^{Cre}$ x $PTEN^{fl/fl}$ x $R26^{tdTomato}$)[106], and ASC Citrine-reporter mice[107] have been described before. Murine cells were either used as a mixture of peritoneal cells directly *ex vivo* by flushing the peritoneal cavity with 5 ml of PBS or as bone marrow-derived macrophages (BMDMϕ)s, which were differentiated from bone marrow cells with murine M-CSF (Immunotools) as described for human macrophages. 8×10^4 peritoneal cells were seeded per well into 96-well plates and left to attach for 2 h at 37 °C, 5% CO_2. Their medium was exchanged afterwards to reduce the amount of non-adherent cells for imaging. BMDMϕs were seeded as 4×10^4 cells per well into 96-well plates after detachment.

For *in vivo* assessment, 8 to 12-week-old age- and sex-matched C57BL/6J wildtype mice (Janvier Labs) were used. Animals received 400 µl containing 2×10^7 heat-killed yeast, 2×10^6 heat-killed hyphae, or an equal volume of PBS as a control via intraperitoneal (*i.p.*) injection. After 24 h, mice were analyzed for weight loss and facial body temperature was measured with an infrared thermometer. Blood was drawn from the retro-bulbar sinus for serum to measure cytokines by ELISA and blood cell composition was determined with a hematological analyzer (Element HT5; Heska). After euthanasia, the peritoneal cavity was flushed with 5 ml PBS containing 2 mM EDTA and isolated cells were analyzed by flow cytometry. Animal experiments were approved by the Austrian Ministry of Sciences (project number 2024-0.796.083) and conducted in accordance with FELASA guidelines.

Macrophage supernatant generation for neutrophil priming

To generate macrophage supernatants for neutrophil priming, 5×10^6 M-CSF-MDMϕs were stimulated with 10^6/ml HKY or 10^5/ml HKH or left unstimulated in 75 cm^2 flasks containing 15 ml RPMI for 24 h. Supernatants were harvested by sterile filtration through 0.2 µm filters and used within one week. Human primary neutrophils were primed in 50% macrophage supernatant mixed with fresh RPMI for 2 h.

Flow cytometry

2×10^5 Neutrophils per well were incubated in 50% macrophage supernatant in 96-well round bottom plates to facilitate direct staining. After 2 h at 37 °C, 5% CO_2, neutrophils were spun down at 300xg, washed in cold FACS buffer (2% FCS in PBS) and incubated with TruStain FcX Fc-Receptor Block 1:20 (Biolegend) for 5 min on ice. Afterwards, cells were spun down again, now at 4 °C, and an antibody mix against CD11b-BV421 (ICRF44), CD15-APC-Fire750 (W6D3), CD16-PerCP-Cy5.5 (3G8), CD35-FITC (E11), CD62L-AlexaFluor647 (DREG-56), CD66b-PE (G10F5), and CD182-PE-Cy7 (5E8, all from Biolegend) for surface staining of activation markers was added for 20 min, 4 °C in the dark. Fixable Viability Dye eFluor506 (Invitrogen) was used to exclude dead cells. Cells were washed with cold FACS buffer and filtered through a 70 µm mesh (Sefar) before acquisition on a BD Biosciences FACSVerse Cell Analyzer flow cytometer. Panel was designed following previous publications.[74, 87, 108, 109]

10^6 M-CSF-MDMϕs or GM-CSF-MDMϕs per well were seeded in 6-well plates in 5 ml per well, rested overnight, washed once with RPMI on the next day and stimulated with 5 ml 10^6/ml HKY or 10^5/ml HKH or left unstimulated with RPMI only. After 90 min, medium was carefully aspirated and cells were incubated in 10 mM EDTA in PBS on ice for 20 min. From now on until fixation, every step was performed on ice. Macrophages were collected by gently scraping and pipetting up and down and washed in FACS buffer with 2 mM EDTA. Cells were afterwards transferred to a V-bottom plate, where Fc-Block, Viability Dye and surface staining mix against HLA-DR-APCefluor780 (L243, Invitrogen), Mincle-AlexaFluor488 (2455C, RD Systems), Dectin-1-PerCP-Cy5.5 (15E2), CD11b-BV650 (ICRF44, both Biolegend), CD206-BV786 (19.2) and CD11c-BUV395 (B-ly6, both BD Biosciences) were added

analogous to neutrophil staining. Cells were washed once with FACS buffer with EDTA and twice with PBS and then fixed and permeabilized according to the instructions of the RD Systems fixation and permeabilization kit. The intracellular staining mix against phospho-AKT-PE (545007, RD Systems), phospho-FAK-AlexaFluor647 (K73-480, BD Biosciences), TNF-PECy7 (Mab11, Invitrogen) and GM-CSF-PEDazzle594 (BVD2-21C11, Biolegend) was added in permeabilization buffer for 30 min at 4 °C in the dark, after which samples were washed with the same buffer and resuspended in FACS buffer with EDTA. Before acquisition on a BD Biosciences LSR Fortessa II, samples were filtered through a 70 µm mesh.

Peritoneal mouse cells were centrifuged at 400×g for 5 min and counted on a BioRad T20 cell counter with Trypan Blue to assess relative viability. By including the recovered volume, absolute live cell numbers could be calculated. Up to 2×10^6 cells per well were treated with Fc-Block (Biolegend) and surface stained against CD11b-PECy7 (M1/70, Invitrogen), Siglec-F-BV421 (E50-2440, BD Biosciences), CD45.2-BV650 (104), Ly6G-AlexaFluor700 (1A8), F4/80-BV605 (BM8), Ly6C-BV510 (HK1.4) and TIM-4-PerCP-Cy5.5 (RMT4-54, all Biolegend) in FACS buffer with EDTA in V-bottom plates as described above. Fixable Viability Dye eFluor780 (Invitrogen) was used to exclude dead cells. Cells were measured on a Beckman-Coulter Cytoflex S. All resulting data were analyzed with FlowJo V10 (BD).

Neutrophil effector functions

For ROS measurements, 2×10^5 human neutrophils were seeded per well in a 96-well plate in 50% macrophage supernatant, total volume of 100 µl, and preincubated for 2 h. 50 µl of 6 h RPMI grown live SC5314 hyphae were added afterwards to reach 5×10^4 hyphae per well. To start the assay, 50 µl of a luminol-HRP (Fluka/Sigma-Aldrich) mixture (400 µM, 32 U/ml) were added and the plate immediately put in a Tecan Infinite reader set to 37 °C to measure luminescence every 2.5 min for 3 h. To assess hyphal killing by neutrophils, 10^5 neutrophils were preincubated for as for the ROS assay. $4\text{x}10^4$ *C. albicans* hyphae, pre-grown as for the ROS assay, were added per well. After 3 h, neutrophils were lysed three times with cold water and washed away. The surviving fungus was incubated with

0.5 mg/ml XTT (Fluka) and 4 µM Menadione (Sigma-Aldrich) for 2 h at 37 °C, 5% CO_2 to develop the formazan chromophore from the XTT by remaining fungal mitochondrial activity. After 2 h, the plate was centrifuged and 100 µl of the supernatant transferred and absorbance measured in a plate reader at 490 nm wavelength with 660 nm reference.

Chemotaxis assay

Neutrophil chemotaxis was based on a published method.[74] Briefly, 2×10^4 human umbilical cord vein endothelial cells (HUVECs) per insert were seeded on Collagen IV-coated 3 µm pore size transwells (Sarstedt) and allowed to reach confluency over 2 days culture in Endothelial cell medium (ECM, PromoCell). On the day of the experiment, freshly isolated human neutrophils were stained with Cytopainter Green (Abcam) (2 µl/ml and 10^6 cells) for 10 min, 4 °C in the dark, washed with HBSS including HEPES pH 7 and resuspended in RPMI. Transwells were moved into a 24-well plate containing 600 µl 50% macrophage supernatants in the bottom compartment. 200 µl of 10^5 stained neutrophils were added to the top compartment and allowed to migrate for 2 h at 37 °C, 5% CO_2. Afterwards, transwells were discarded and the bottom compartment was imaged for green fluorescence at 6 positions per well in a Cell Discoverer 7 (Zeiss). Quantification was performed via Fiji[110] and normalized to counts from wells, where neutrophils were added directly without transwells as 100%.

Proteome preparation and enrichment analysis

Proteins from sterile-filtered macrophage supernatants were concentrated over 10 kDa molecular weight cut-off (MWCO) filters and stored at -80 °C until further preparation. Trifluorethanol (TFA) was added 1:1 to denature the proteins. Further, 2 µL per 100 µl of 500 mM tris(2-carboxyethyl)phosphine (TCEP) and 625 mM 2-chloroacetamide (CAA) solubilized in 50 mM triethylammonium bicarbonate (TEAB) were added and incubated at 70 °C for 30 min to reduce and carbamidomethylate proteins. Proteins were precipitated with methanol/chloroform/H_2O[111] and resolubilized in 100 mM TEAB in 5:95 TFE/H_2O (v/v), and digested for 18 h at 37°C after addition of Trypsin/Lys-C mix at a protease-to-

protein proportion of 4%. Samples were dried with a vacuum concentrator, resolved in 30 µl 0.05% TFA in H_2O/Acetonitril 98:/2 (v/v) and run over a 10 kDa PES membrane MWCO to analyse the filtrate via an Ultimate 3000 nano RSLC system connected to a QExactive HF mass spectrometer (both Thermo Fisher Scientific, Waltham, MA, USA) LC-MS/MS setup. Peptide trapping for 5 min on an Acclaim Pep Map 100 column (2 cm x 75 µm, 3 µm) at 5 µL/min was followed by separation on an analytical Acclaim Pep Map RSLC nano column (50 cm x 75 µm, 2µm). Mobile phase gradient elution of eluent A (0.1% (v/v) formic acid in water) mixed with eluent B (0.1% (v/v) formic acid in 90/10 acetonitrile/water) was performed using the following gradient: 0-5 min at 4% B, 30 min at 7% B, 60 min at 10% B, 100 min at 15% B, 140 min at 25% B, 180 min at 45% B, 200 min at 65% B, 210-215 min at 96% B, 215.1-240 min at 4% B. Positively charged ions were generated at spray voltage of 2.2 kV using a stainless steel emitter attached to the Nanospray Flex Ion Source (Thermo Fisher Scientific). The quadrupole/orbitrap instrument was operated in Full MS / data-dependent MS2 mode. Precursor ions were monitored at m/z 300-1500 at a resolution of 120,000 FWHM (full width at half maximum) using a maximum injection time (ITmax) of 120 ms and an AGC (automatic gain control) target of 3×10^6. Precursor ions with a charge state of z=2-5 were filtered at an isolation width of m/z 4.0 amu for further fragmentation at 28% HCD collision energy. MS2 ions were scanned at 15,000 FWHM (ITmax=100 ms, AGC= 2×10^5).

Protein database search: Tandem mass spectra were searched against the UniProt databases of *Homo sapiens* (https://www.uniprot.org/proteomes/UP000005640) from 2022/11/04 (YYYY/MM/DD) using Proteome Discoverer (PD) 3.0 (Thermo) and the database search algorithms Mascot 2.8, Comet, MS Amanda 2.0, Sequest HT with and without INFERYS Rescoring and MSPepSearch (spectral library from NIST, human_hcd) with Precursor Detector node. Two missed cleavages were allowed for the tryptic digestion. The precursor mass tolerance was set to 10 ppm and the fragment mass tolerance was set to 0.02 Da. Modifications were defined as dynamic Met oxidation, phosphorylation of Ser, Thr, and Tyr, protein N-term acetylation with and without Met-loss as well as static Cys carbamidomethylation. A strict false discovery rate (FDR) < 1% (peptide and protein level) was required for positive protein hits. Furthermore, specific search engine scores of Mascot (>30), Sequest HT and Comet (>3), MS

Amanda (>300), MS PepSearch (>600) or CHIMERYS (>2) were required. The Percolator node of PD3.0 and a reverse decoy database was used for q-value validation of spectral matches. Only rank 1 proteins and peptides of the top scored proteins were counted. Label-free protein quantification was based on the Minora algorithm of PD3.0 using the precursor abundance based on intensity and a signal-to-noise ratio >5. Normalization was performed by using the total peptide amount method. Imputation of missing quan values was applied by using abundance values of 75% of the lowest abundance identified per sample.

GO term enrichment was performed on 28th of February 2024 using the online **G**ene **O**ntology en**RI**chment ana**L**ysis and visua**L**iz**A**tion tool (GOrilla).[44, 45] GO-term enrichment was performed with a *p*-value threshold of 10^{-3}, in the ontology categories "Biological process" and "Cellular component". Subsequently, Gene Ontology term lists were summarized by removing redundant GO terms with REVIGO[112] using *C*=0.4, and GO terms with less than 3 genes associated were removed.

Enzyme-linked Immunosorbent Assay (ELISA)

ELISA from cell culture supernatants of 4×10^4 macrophages per well from 96-well plates and the serum of mice was performed according to the instructions of the RD Systems Duoset Kits.

(Live-cell) Microscopy and analysis

4×10^4 human MDMϕs, 10^5 PBMCs or 10^5 $CD14^+$ monocytes were seeded in 96-well plates. Macrophages were seeded the day before and rested, PBMCs and monocytes allowed 2 h to settle down. Adherent cells were gently washed once and their medium replaced with 100 µl RPMI containing 2 µM SytoDeepRed, 1 µM SytoxGreen (both Invitrogen). In some experiments additionally 5 µM CellRoxOrange (Invitrogen) was included at this step. Cells were preincubated at 37 °C, 5% CO_2 for 45 min for SytoDeepRed to diffuse into live cell nuclei. In some experiments, at this step, blocking antibodies against Mincle (15H5), Dectin-1 (22H8, both Invivogen), CD11b (M1/70, BioXcell / 2LPM19c, Thermo Fisher) and their corresponding isotype controls at 10 µg/ml concentration or diverse

inhibitors all from Invivogen, except PF-573228, N-acetyl-cysteine, DPI, GW5074, Z-VAD-FMK (all Sigma-Aldrich) and Duvelisib (Selleckchem) at specified concentrations in the corresponding figure legends or their DMSO solvent control (AppliChem) were added. Afterwards 100 µl fungal stimuli or RPMI were added to a final volume of 200 µl and cells were imaged for phase contrast, green, near-infrared (and orange) fluorescence on a Zeiss Cell Discoverer 7 or a Sartorius Incucyte S3 or SX5 under cell culture conditions for 24 h, unless indicated otherwise. Mouse macrophages were not stained with SytoDeepRed, as we could not achieve homogeneous labeling in those cells. Mouse cells further were cultured with 1x Penicillin/Streptomycin (Gibco). To circumvent poor survival of unstimulated mouse macrophages in serum-free medium, we included 10 ng/ml M-CSF during all mouse macrophage experiments. Imaging quantification was performed with Fiji or the Incucyte Software (Sartorius). Briefly, to track cell death kinetics, the count of SytoxGreen positive events (dead cells) over time was normalized to the initial count of SytoDeepRed (all cells) of the same well and position to calculate the individual percentage cell death over time (% nuclear stain^{+}). Cell death kinetics of LysM^{Cre} x PTEN$^{fl/fl}$ x R26^{tdTomato} macrophages were enumerated by calculating the difference between the number of Tomato^{+} cells over time (Count t_x) relative to the initial count (Count t_0 = 100%) in the same well. This was followed by a normalization to the corresponding unstimulated cells leading to the following formula: % Hyphoptosis = (Count t_0 -(Stimulated Count Tomato t(x)/Stimulated Count Tomato t_0) -(Count t_0 -(unstimulated Count Tomato t(x)/unstimulated Count Tomato t_0)). The Fiji Macro and the Incucyte analysis definitions can be shared upon request. For non-fluorescent mouse cells, a high control well was included for each biological replicate, where 100% cell death was achieved by adding 15 µl 70% EtOH, which was used to normalize on. CellRoxOrange bulk data were analyzed by multiplying the mean fluorescence intensity with the positive area of an image to retrieve the integrated intensity (Int Int) and normalized to the initial SytoDeepRed count (Int Int/cell). This was calculated for each time point and the area under the curve was retrieved (AUC Int Int over t/cell). For single cell tracking, images were blinded and individual cells were manually followed from their moment of death (becoming SytoxGreen^{+}), back in time to the time point, when they lost their

cytosolic CellRoxOrange signal. The time differences between those two events were calculated for (where possible) 50 individual cells from two image series per donor and condition. To visualize inflammasome assembly, $6x10^4$ ASC-reporter BMDMϕs were seeded in Ibidi chamber slides the day before the experiment. Some conditions were primed with 50 ng/ml LPS for 2 h before adding HKH. Cells were fixed 5 h later with 4% Histofix (Roth, Karlsruhe, Germany) for 20 min, washed with PBS and imaged on a Zeiss Observer microscope for citrine-labeled ASC specks.

Dual Killing assay

To assess the antifungal capacity of immune cells in real-time, we set up a live-cell imaging "dual killing assay", in which we can in parallel dynamically measure host cell death via SytoxGreen$^+$ events and immune cell-permitted fungal hyphal outgrowth in an Incucyte SX5 (Sartorius). This is achieved by using a fluorescent *C. albicans* strain (SC5314 mScarlet[113]) and the Neurotrack analysis tool[114] for fluorescence of the Incucyte software. Analysis definitions will be shared upon request.

Genetic association study and eQTL datasets

To investigate genetic variants linked to candidemia susceptibility within specific gene regions, we utilized a previously published GWAS of candidemia.[75] After quality control, 178 patients and 175 matched controls underwent genome-wide association studies (GWAS). We performed the association analysis using Fisher's test with PLINK V1.9 software.[115] Association results for the chromosomal regions of candidate genes were extracted and visualized using the LocusZoom tool.[116] To investigate the functional consequences of genetic polymorphisms within these gene regions, we integrated expression quantitative trait loci (eQTL) data, retrieved on the 7th of January 2025, from the eQTLGen Phase I database.[78]

Data analysis and statistics

Most data were analyzed with GraphPad Prism V10, unless indicated otherwise. Normal distribution was tested with Shapiro-Wilk test. Depending on the setup, the number of potential sources of variation and if the same individual was tested under different conditions, afterwards (paired) t-test for 2 groups, One-Way ANOVA for more than 2 groups and one source of variation or Two-Way-ANOVA for more than 2 groups and 2 sources of variation, were applied to determine statistically significant differences. In case of non-normal distribution, Mann-Whitney/Wilcoxon, Kruskal-Wallis/Friedman tests were used instead of t-test and One-Way-ANOVA. Holm-Šídák or Dunn's post-hoc tests were applied, accordingly. See figure legends for specific testing method.

Resource availability

Lead contact

Requests for further information and resources should be directed to and will be fulfilled by the lead contact Mark S. Gresnigt (mark.gresnigt@leibniz-hki.de).

Materials availability

No new unique reagents have been generated in this study.

Data and code availability

The mass spectrometry proteomics data have been deposited to the ProteomeXchange Consortium via the PRIDE[117] partner repository with the dataset identifier PXD058866. No new code has been generated specifically for this study.

Acknowledgements

The authors acknowledge Bernhard Hube (Microbial Pathogenicity Mechanisms "MPM", Leibniz-HKI) and Axel A. Brakhage (Molecular and Applied Microbiology, Leibniz-HKI) for fruitful discussions, their mentorship and generous sharing of laboratory infrastructure. We would like to thank Ilse D. Jacobsen

and Marie von Lilienfeld-Toal for providing access to flow cytometers. We thank Christoph Becker for sharing *Gsdmd* knockout bone marrow and Kerstin Voigt for gifting strains of filamentous fungi. We want to further thank the great team at Adaptive Pathogenicity Strategies ("APS", Leibniz-HKI) and particularly all the supportive members of the macrophage team from APS and MPM. Additionally, we would like to specifically acknowledge Sophie Austermeier, Larsen Vornholz, Denis de Graaf, Josefine Lehmann, Monia Camboni and Nadja Jablonowski for their organizational and technical support, Lydia Kasper for an introduction on imaging host-fungal interactions and its quantification, Osama Elshafee for continued constructive criticism on the project, and Stefanie Westermann for critical reading of the manuscript. Lastly, we thank all volunteers, who donated their blood for this study.

Funding

This work was funded by the Deutsche Forschungsgemeinschaft (DFG, German Research Foundation) Emmy Noether Program (project no. 434385622 / GR 5617/1-1) to MSG and DFG Collaborative Research Center/Transregio FungiNet 124 (project Z2 and A1; project number 210879364) to MSG and OK. This work (AD) was further supported by an Exploration Grant of the Boehringer Ingelheim Foundation (BIS) to MSG and a European Society of Clinical Microbiology and Infectious Diseases (ESCMID) research grant to AD. This research was supported by the Free State of Thuringia and co-funded by the European Union – Project-ID 2023 FGI 0004. "A Live broadcast of the interactions between host and fungal pathogens" to MSG and AD.

Author Contributions Statement

Conceptualization: AD, MSG

Methodology: AD, LM, TK, CKB, MV, OK, VK, MSG

Investigation: AD, LM, TK, MH

Validation: SD, FB

Formal Analysis: AD, TK, CKB, CO, VK, MSG

Resources: SW, EL, JR, GS

Data Curation: AD, LM, TK, CKB, MSG

Visualization: AD, MSG

Writing - Original draft: AD, TK, CKB, MSG

Writing - Review and editing: AD, LM, TK, CKB, FB, MV, OK, VK, MSG

Supervision: AD, VK, GS, MSG

Project administration: AD, LM, OK, VK, GS, MSG

Funding Acquisition: AD, OK, VK, GS, MSG

Competing Interest Statement

The authors declare no competing interests.

Supplementary figures:

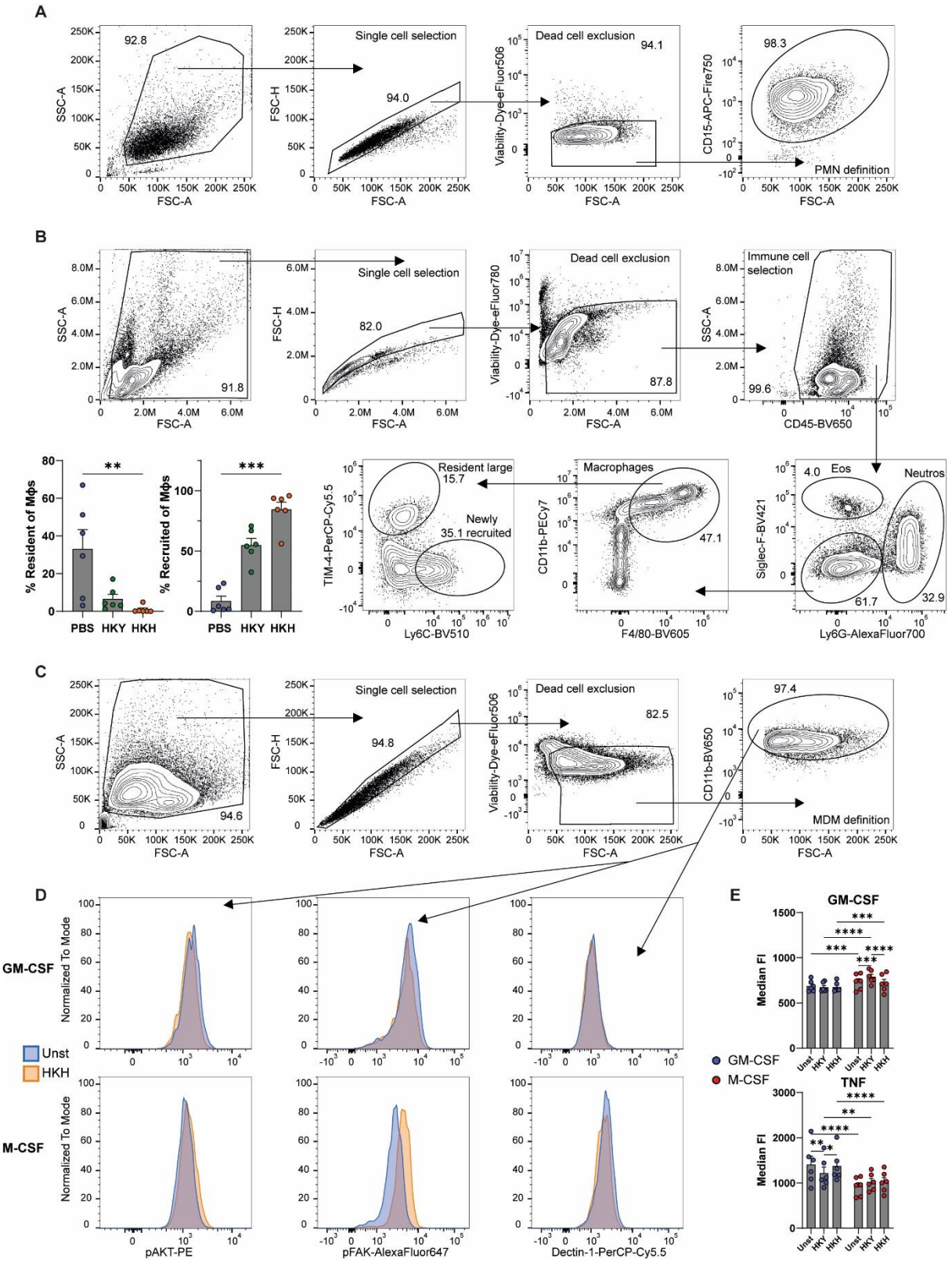


Figure S1: Gating strategies for flow cytometry. (A) Exemplary FACS plots for definition of human neutrophils isolated from peripheral blood after *in vitro* stimulation. After single cell selection and exclusion of dead cells, neutrophils were defined as the CD15⁺ population, from which MFIs of activation markers were assessed. **(B)** Gating scheme for mouse peritoneal cells. After single cell selection and dead cell exclusion, immune cells were selected by CD45⁺ staining. From this population,

eosinophils (Siglec-F$^+$ / LyG6$^-$) and neutrophils (Ly6G$^+$) were defined. From the double negative population, the total macrophage population was defined by CD11b$^+$ / F4/80$^+$. Macrophages were further discriminated into large resident macrophages (TIM-4$^+$ / Ly6C$^-$) and newly recruited macrophages (TIM-4$^-$ / Ly6C$^+$), of which the distribution quantification among macrophages is displayed as the mean + SEM of 6 mice per group. Statistically significant differences were determined by One-Way ANOVA against PBS control group with Holm-Šídák post-hoc testing. **(C)** Exemplary FACS plots for definition of human macrophages (*in vitro* differentiated monocyte-derived). After single cell selection and exclusion of dead cells, total macrophages were defined as the CD11b$^+$ population. **(D)** Representative histograms of selected molecules implicated in inflammatory macrophage cell death, that were regulated by stimulation with hyphae in M-CSF-dependent, but not GM-CSF-dependent macrophages after 90 min. Dectin-1 was surface-stained, pAKT and pFAK intracellularly. For quantification and statistical analysis, see main figure 6 F, G. **(E)** Median fluorescence intensities of intracellular cytokines corresponding to main figure 6 F, G. Significance levels *p < 0.05, **p < 0.01, ***p < 0.001, ****p < 0.0001.



Figure S2: Dead hyphae are toxic to macrophages even in absence of candidalysin. Live-cell imaging with SytoxGreen to visualize cell death kinetics in human MDMϕ triggered by HKH of candidalysin-deficient *Ece1-/- C. albicans*. MOI 0.5; percentage cell death was calculated by normalizing SytoxGreen$^+$ counts to initial total nuclei count. Data are pooled from 4 biologically different macrophage donors and shown as mean + SEM. Statistically significant differences were determined by Repeated-Measurements Two-Way ANOVA and Holm-Šídák post-hoc test with displayed significance symbols in the graph representing the most significant p-value reached in the indicated time frame of consecutive measurements "t". Significance levels ****p < 0.0001

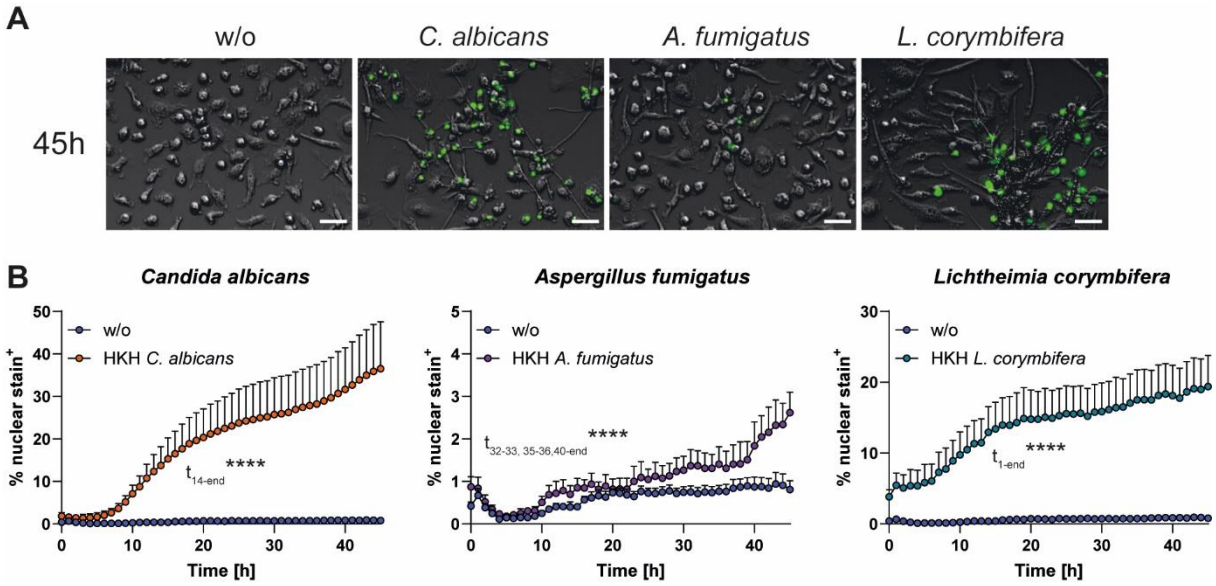


Figure S3: Dead hyphae of other fungal pathogens also induce cell death in human macrophages. Live-cell imaging with SytoxGreen to visualize cell death kinetics in human MDMϕ triggered by HKH of indicated fungal species. **(A)** Representative images and **(B)** quantification of macrophage death over time; MOI 0.5; Percentage of cell death was calculated by normalizing SytoxGreen$^+$ counts to initial total nuclei count. Scale bars represent 25 µm. Data are pooled from 4 biologically different macrophage donors and shown as mean + SEM. Statistically significant differences were determined by Repeated-Measurements Two-Way ANOVA and Holm-Šídák post-hoc test with displayed significance symbols in the graph representing the most significant p-value reached in the indicated time frame of consecutive measurements "t". Significance levels ****p < 0.0001

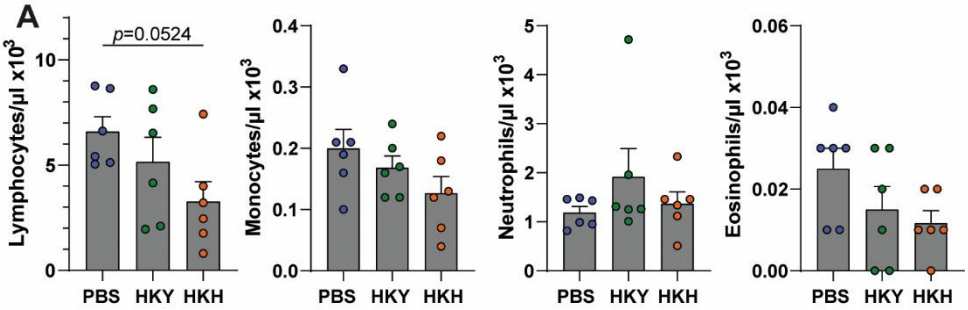


Figure S4: White blood cell composition of mice after *i.p.* injection. (A) Cell-type specific counts of mouse blood 24 h after the indicated *i.p.* injection, measured with a haematological analyser. Data are pooled from 6 mice per group, shown as mean + SEM and statistically significant differences were determined with One-Way ANOVA against PBS control group with Holm-Šídák post-hoc test.

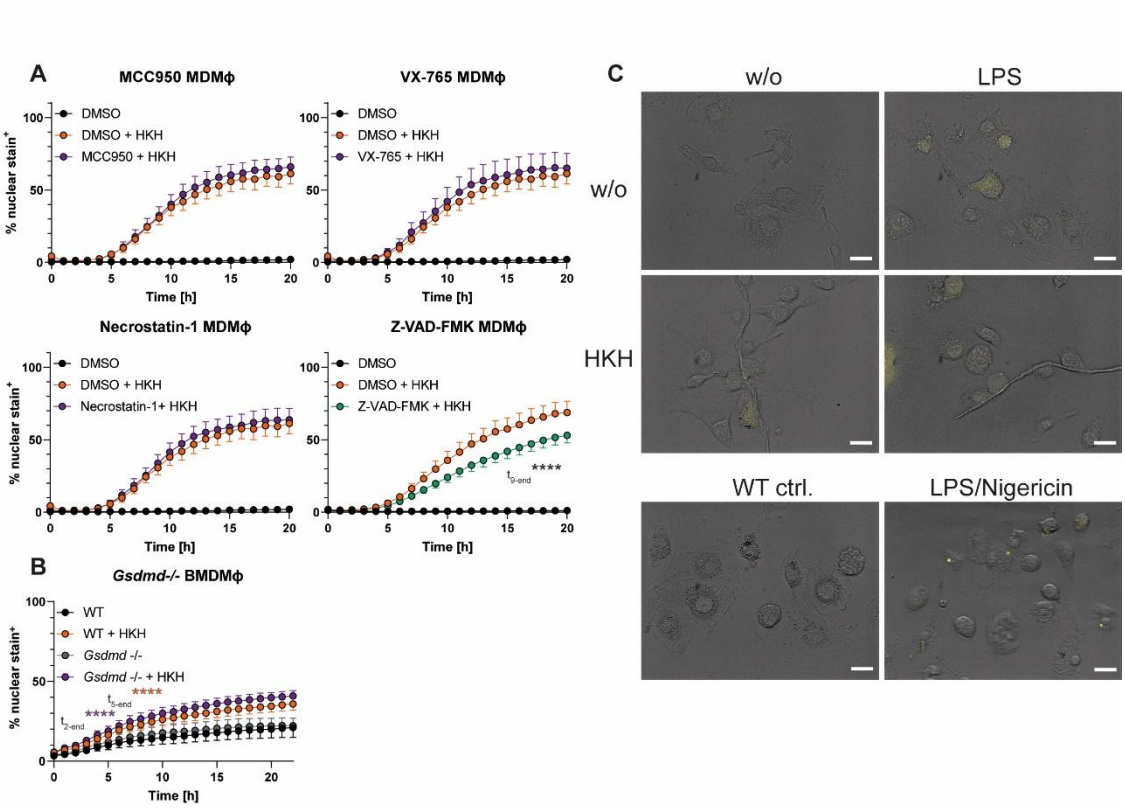


Figure S5: Canonical pyroptosis and necroptosis are likely not involved in hyphae-induced inflammatory macrophage cell death. (A) Cell death kinetic analysis of MDMϕs treated with SC5314 HKH in presence of the indicated inhibitors, including a 45 min preincubation: 200 nM MCC950 (NLRP3 inflammasome), 10 µM VX-765 (pyroptotic caspases), 20 µM Necrostatin-1 (RIPK1-RIPK3, necroptosis) or 25 µM Z-VAD-FMK (pan-Caspase). SytoxGreen+ events over time were normalized to initial total number of cells per image to calculate percentages of cell death. Data are displayed as the mean + SEM and pooled from 7 (8 for Z-VAD-FMK) biologically different macrophage donors. **(B)** Cell death kinetic analysis of WT and *Gsdmd-/-* BMDMϕs stimulated with HKH or left unstimulated. Scale bars represent 20 µm. Data show mean + SEM and are pooled from 4-5 mice per group. Percentages were calculated according to high control well with complete lysis. **(C)** R26-CAG-ASC-citrine reporter BMDMϕs were screened for ASC speck formation after 5 h hyphae stimulation +/- priming with 50 ng/ml LPS for 2 h with Nigericin 1.5 µM as positive control from one BMDMϕ culture. Displayed significance symbols in the cell death kinetics represent the most significant *p*-value reached in the indicated time frame of consecutive measurements "t" with coloured symbols indicating comparisons of correspondingly coloured treatment group against untreated. Significance levels ****$p <$ 0.0001.

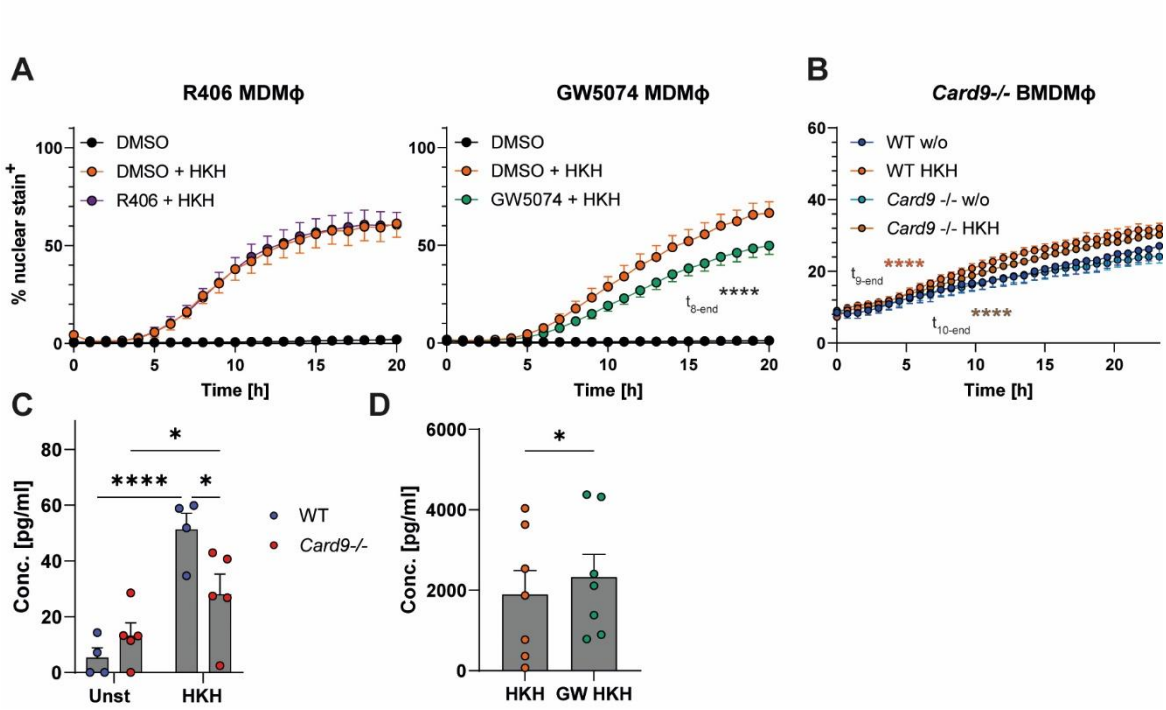


Figure S6: Downstream effects of Dectin-1 split into SYK-CARD9 for inflammation and Raf-1 for cell death induction. (A) Cell death kinetic analysis of MDMϕs treated with SC5314 HKH in presence of the indicated inhibitors, including a 45 min preincubation: 2 µM R406 (SYK), 20 nM GW5074 (Raf-1). Data are pooled from 7 (SYK) or 12 (Raf-1) biologically different macrophage donors. SytoxGreen+ events over time were normalized to initial total number of cells per image to calculate percentages of cell death. **(B)** Cell death kinetic analysis of WT and *Card9-/-* BMDMϕs stimulated with HKH or left unstimulated. Data are pooled from 4-5 mice per group. Percentages were calculated according to high control well with complete lysis. **(C)** TNF ELISA from supernatants of mouse WT and *Card9-/-* BMDMϕs stimulated with HKH for 24 h, pooled from 4-5 mice per group. **(D)** TNF ELISA from supernatants of human MDMϕs stimulated with HKH for 24 h, pre-treated with 20 nM GW5074 or solvent control. Data are pooled from 7 biologically different macrophage donors. Data are shown as mean + SEM, with bar graphs showing individual biological replicates as dots. Statistically significant differences were determined by **(C)** Two-Way-ANOVA or **(A, B)** repeated measurement Two-Way ANOVA and Holm-Šídák post-hoc test or **(D)** a paired t-test. Displayed significance symbols in the cell death kinetics represent the most significant *p*-value reached in the indicated time frame of consecutive measurements "t" with the coloured symbols indicating the comparison of the correspondingly coloured treatment group against untreated. Significance levels **p* < 0.05, *****p* < 0.0001.

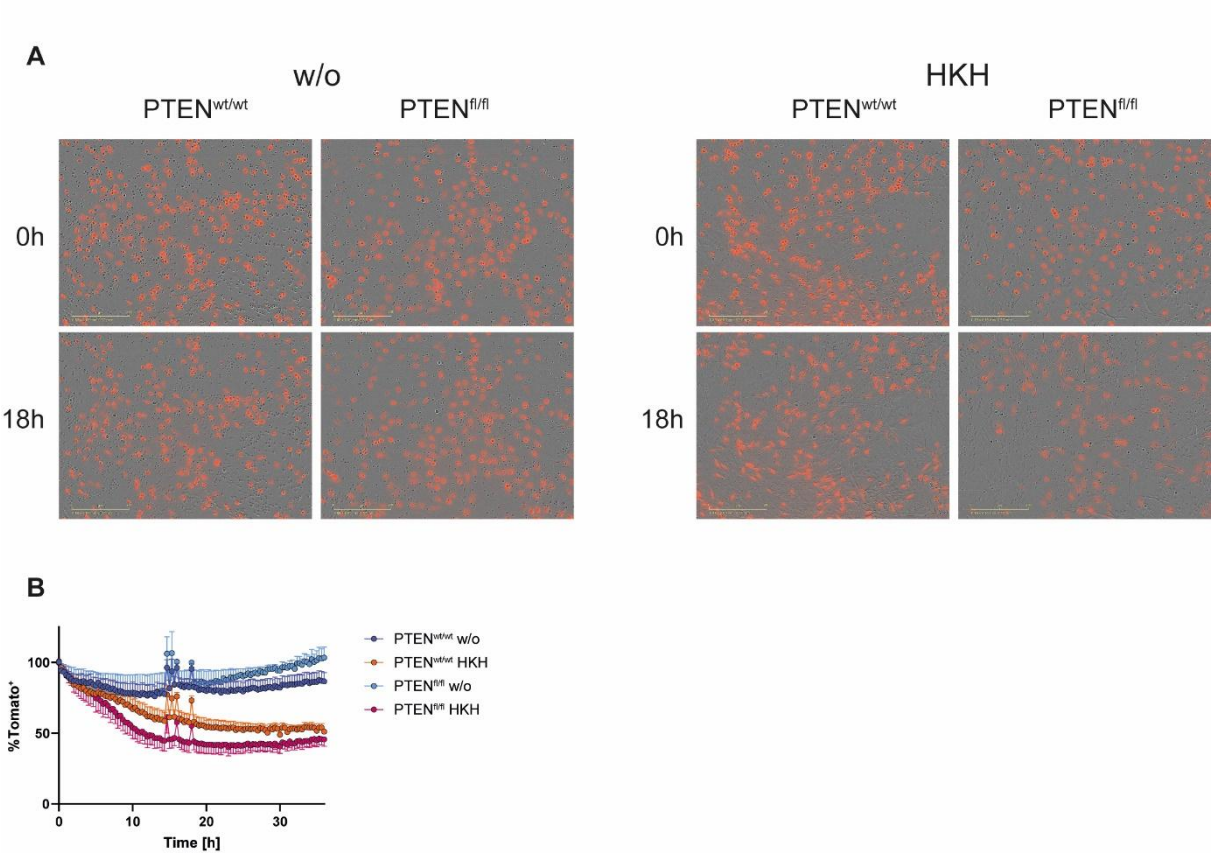


Figure S7: Microscopy of PTEN-deficient mouse peritoneal cells. (A) Representative images of peritoneal cells from LysM^{Cre} x PTEN$^{fl/fl}$ x R26^{tdTomato} and corresponding LysM^{Cre} x PTEN$^{wt/wt}$ x R26^{tdTomato} mice treated with 10^5/ml HKH or left unstimulated at 0 h and 18 h post stimulation. **(B)** Kinetic quantification of Tomato$^+$ cell number normalized to initial Tomato$^+$ cell count to compare relative loss of LysM-expressing cells over time between genotypes and stimulations. Data are pooled from 4-6 mice per group.

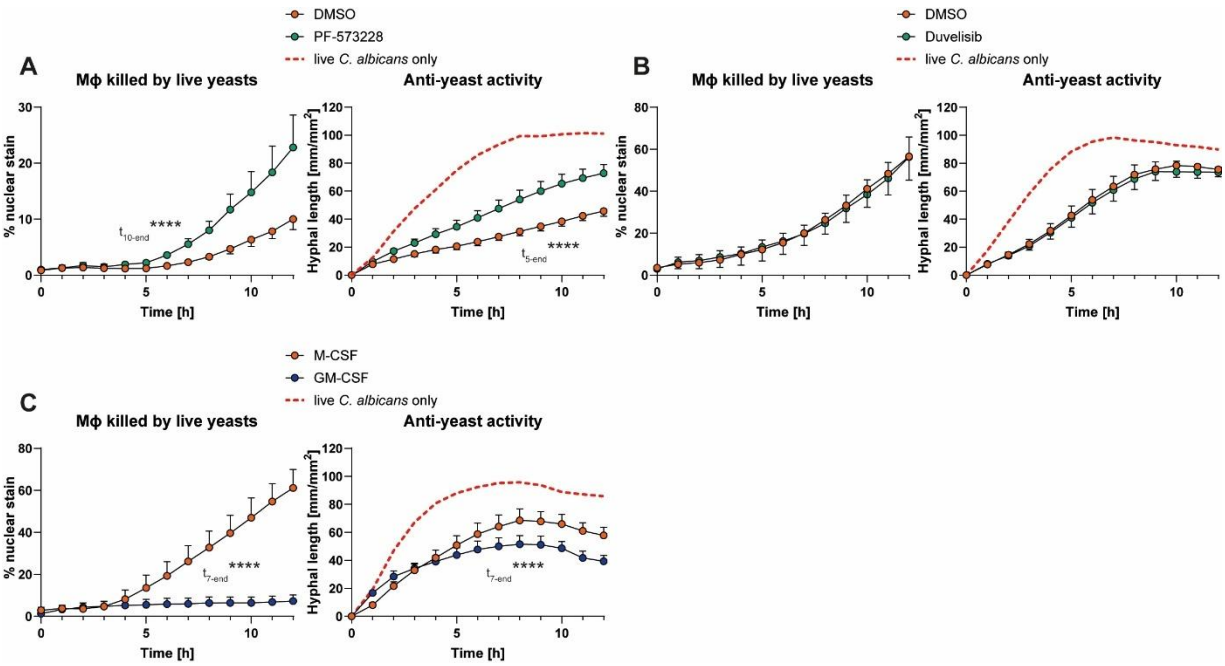


Figure S8: Hyphoptosis-inhibiting treatments modulate macrophage performance against yeast morphology encounters. hMDMϕs were confronted with viable SC5314-mScarlet yeasts (MOI 2.5) and followed by live-cell imaging. Mϕ death kinetics

(SytoxGreen$^+$) and (Mϕ-)permitted hyphal outgrowth quantification over time ("dual killing assay") under hyphoptosis-inhibiting conditions via **(A)** 10 µM PF-573228 (5 donors), **(B)** 200 nM Duvelisib (4 donors), **(C)** alternative differentiation with GM-CSF (5 donors). Displayed significance symbols in the cell death kinetics represent the most significant *p*-value reached in the indicated time frame of consecutive measurements "t". Significance levels *$p < 0.05$, **$p < 0.01$, ****$p < 0.0001$.

Supplementary video S1: Live-cell imaging overview of dynamic cell death induction by fungal hyphae. 4x10^4 human MDMϕs were either unstimulated or treated with 2x10^5 HKY or 2x10^4 HKH of *C. albicans* and live-cell microscopy monitored for cell death induction by green fluorescence via SytoxGreen over the course of 24 h. Corresponding to main Figure 1.

Supplementary video S2: Zoom on live-cell imaging of dynamic cell death induction by fungal hyphae. 4x10^4 human MDMϕs were treated with 2x10^5 HKY or 2x10^4 HKH of *C. albicans* and live-cell microscopy monitored for cell death induction by green fluorescence via SytoxGreen over the course of 24 h. Corresponding to main Figure 1.

Supplementary video S3: Comparison of hyphoptosis induction between regular macrophages and multinucleated giant cells. 9 days after starting enrichment of giant cells from 4x10^4 differentiated human MDMϕs, the enriched populations (M-CSF + IL-4) or control macrophages (M-CSF only) were treated with 2x10^4 HKH of *C. albicans* and live-cell microscopy monitored for cell death induction by green fluorescence via SytoxGreen over the course of 24 h. SytoDeepRed (red fluorescence) was additionally implemented to visualize multinucleated status of giant cells. Corresponding to main Figure 4.

References

1. WHO (2022).
2. Brown, G.D. *et al.* The pathobiology of human fungal infections. *Nature Reviews Microbiology* **22**, 687–704 (2024).
3. Lo, H.J. *et al.* Nonfilamentous C. albicans mutants are avirulent. *Cell* **90**, 939–949 (1997).
4. Nucci, M. & Anaissie, E. Fusarium Infections in Immunocompromised Patients. *Clinical Microbiology Reviews* **20**, 695–704 (2007).
5. Kauffman, C.A. Histoplasmosis: a Clinical and Laboratory Update. *Clinical Microbiology Reviews* **20**, 115–132 (2007).
6. Estrada, R., Chávez-López, G., Estrada-Chávez, G., López-Martínez, R. & Welsh, O. Eumycetoma. *Clin Dermatol* **30**, 389–396 (2012).
7. Ibrahim, A.S., Spellberg, B., Walsh, T.J. & Kontoyiannis, D.P. Pathogenesis of Mucormycosis. *Clinical Infectious Diseases* **54**, S16–S22 (2012).
8. Chen, Y.-L. *et al.* Calcineurin Controls Hyphal Growth, Virulence, and Drug Tolerance of Candida tropicalis. *Eukaryotic cell* **13**, 844–854 (2014).
9. Tischler, B.Y. & Hohl, T.M. Menacing Mold: Recent Advances in Aspergillus Pathogenesis and Host Defense. *Journal of Molecular Biology* **431**, 4229–4246 (2019).
10. Arévalo-Jaimes, B.V., Admella, J., Blanco-Cabra, N. & Torrents, E. Culture media influences Candida parapsilosis growth, susceptibility, and virulence. *Front Cell Infect Microbiol* **13**, 1323619 (2023).
11. Brown, J.C. & Ballou, E.R. Is Cryptococcus neoformans a pleomorphic fungus? *Curr Opin Microbiol* **82**, 102539 (2024).
12. Mogavero, S. *et al.* Candidalysin delivery to the invasion pocket is critical for host epithelial damage induced by Candida albicans. *Cellular microbiology* **23**, e13378 (2021).
13. Kumamoto, C.A., Gresnigt, M.S. & Hube, B. The gut, the bad and the harmless: Candida albicans as a commensal and opportunistic pathogen in the intestine. *Current Opinion in Microbiology* **56**, 7–15 (2020).
14. Denning, D.W. Global incidence and mortality of severe fungal disease. *The Lancet. Infectious diseases* (2024).
15. Lionakis, M.S., Drummond, R.A. & Hohl, T.M. Immune responses to human fungal pathogens and therapeutic prospects. *Nature reviews. Immunology* (2023).
16. Lass-Florl, C. *et al.* Invasive candidiasis. *Nat Rev Dis Primers* **10**, 20 (2024).
17. Kadosh, D. Regulatory mechanisms controlling morphology and pathogenesis in Candida albicans. *Current Opinion in Microbiology* **52**, 27–34 (2019).

18. Martin, R. *et al.* A core filamentation response network in Candida albicans is restricted to eight genes. *PLoS One* **8**, e58613 (2013).
19. Moyes, D.L. *et al.* Candidalysin is a fungal peptide toxin critical for mucosal infection. *Nature* **532**, 64–68 (2016).
20. Argimón, S. *et al.* Developmental regulation of an adhesin gene during cellular morphogenesis in the fungal pathogen Candida albicans. *Eukaryotic cell* **6**, 682–692 (2007).
21. Phan, Q.T. *et al.* Als3 is a Candida albicans invasin that binds to cadherins and induces endocytosis by host cells. *PLoS biology* **5**, e64 (2007).
22. Leonardi, I. *et al.* CX3CR1(+) mononuclear phagocytes control immunity to intestinal fungi. *Science (New York, N.Y.)* **359**, 232–236 (2018).
23. Wang, X. *et al.* MAVS Expression in Alveolar Macrophages Is Essential for Host Resistance against Aspergillus fumigatus. *J Immunol* **209**, 346–353 (2022).
24. Austermeier, S., Kasper, L., Westman, J. & Gresnigt, M.S. I want to break free - macrophage strategies to recognize and kill Candida albicans, and fungal counter-strategies to escape. *Curr Opin Microbiol* **58**, 15–23 (2020).
25. Jaeger, M. *et al.* Alpha1-antitrypsin impacts innate host-pathogen interactions with Candida albicans by stimulating fungal filamentation. *Virulence* **15**, 2333367 (2024).
26. Uwamahoro, N. *et al.* The pathogen Candida albicans hijacks pyroptosis for escape from macrophages. *mBio* **5**, e00003–e00014 (2014).
27. Kasper, L. *et al.* The fungal peptide toxin Candidalysin activates the NLRP3 inflammasome and causes cytolysis in mononuclear phagocytes. *Nat Commun* **9**, 4260–4260 (2018).
28. Ding, X. *et al.* Inflammasome-mediated GSDMD activation facilitates escape of Candida albicans from macrophages. *Nat Commun* **12**, 6699 (2021).
29. Olivier, F.A.B. *et al.* The escape of Candida albicans from macrophages is enabled by the fungal toxin candidalysin and two host cell death pathways. *Cell Rep* **40**, 111374 (2022).
30. Briard, B., Malireddi, R.K.S. & Kanneganti, T.-D. Role of inflammasomes/pyroptosis and PANoptosis during fungal infection. *PLoS pathogens* **17**, e1009358 (2021).
31. Swidergall, M. *et al.* Candidalysin Is Required for Neutrophil Recruitment and Virulence During Systemic Candida albicans Infection. *J Infect Dis* **220**, 1477–1488 (2019).
32. Drummond, R.A. *et al.* CARD9(+) microglia promote antifungal immunity via IL-1β- and CXCL1-mediated neutrophil recruitment. *Nat Immunol* **20**, 559–570 (2019).
33. Hopke, A. *et al.* Neutrophil swarming delays the growth of clusters of pathogenic fungi. *Nat Commun* **11**, 2031 (2020).
34. Branzk, N. *et al.* Neutrophils sense microbe size and selectively release neutrophil extracellular traps in response to large pathogens. *Nat Immunol* **15**, 1017–1025 (2014).
35. Bruns, S. *et al.* Production of Extracellular Traps against Aspergillus fumigatus In Vitro and in Infected Lung Tissue Is Dependent on Invading Neutrophils and Influenced by Hydrophobin RodA. *PLoS pathogens* **6**, e1000873 (2010).
36. Bain, J.M. *et al.* Immune cells fold and damage fungal hyphae. *Proceedings of the National Academy of Sciences of the United States of America* **118** (2021).
37. Maxson, M.E. *et al.* Integrin-based diffusion barrier separates membrane domains enabling the formation of microbiostatic frustrated phagosomes. *eLife* **7**, e34798 (2018).
38. Tucey, T.M. *et al.* Glucose Homeostasis Is Important for Immune Cell Viability during Candida Challenge and Host Survival of Systemic Fungal Infection. *Cell Metab* **27**, 988–1006.e1007 (2018).
39. Netea, M.G., van de Veerdonk, F.L., van der Meer, J.W., Dinarello, C.A. & Joosten, L.A. Inflammasome-independent regulation of IL-1-family cytokines. *Annu Rev Immunol* **33**, 49–77 (2015).
40. Berkow, R.L., Wang, D., Larrick, J.W., Dodson, R.W. & Howard, T.H. Enhancement of neutrophil superoxide production by preincubation with recombinant human tumor necrosis factor. *J Immunol* **139**, 3783–3791 (1987).

41. Shalaby, M.R. *et al.* Activation of human polymorphonuclear neutrophil functions by interferon-gamma and tumor necrosis factors. *J Immunol* **135**, 2069–2073 (1985).
42. Djeu, J.Y., Matsushima, K., Oppenheim, J.J., Shiotsuki, K. & Blanchard, D.K. Functional activation of human neutrophils by recombinant monocyte-derived neutrophil chemotactic factor/IL-8. *J Immunol* **144**, 2205–2210 (1990).
43. Lopez, A.F. *et al.* Recombinant human granulocyte-macrophage colony-stimulating factor stimulates in vitro mature human neutrophil and eosinophil function, surface receptor expression, and survival. *The Journal of clinical investigation* **78**, 1220–1228 (1986).
44. Eden, E., Lipson, D., Yogev, S. & Yakhini, Z. Discovering Motifs in Ranked Lists of DNA Sequences. *PLOS Computational Biology* **3**, e39 (2007).
45. Eden, E., Navon, R., Steinfeld, I., Lipson, D. & Yakhini, Z. GOrilla: a tool for discovery and visualization of enriched GO terms in ranked gene lists. *BMC Bioinformatics* **10**, 48 (2009).
46. Miyake, K. *et al.* Single-cell transcriptomics identifies the differentiation trajectory from inflammatory monocytes to pro-resolving macrophages in a mouse skin allergy model. *Nat Commun* **15**, 1666 (2024).
47. Vega-Pérez, A. *et al.* Resident macrophage-dependent immune cell scaffolds drive anti-bacterial defense in the peritoneal cavity. *Immunity* **54**, 2578–2594.e2575 (2021).
48. Gross, O. *et al.* Syk kinase signalling couples to the Nlrp3 inflammasome for anti-fungal host defence. *Nature* **459**, 433–436 (2009).
49. Wellington, M., Koselny, K., Sutterwala, F.S. & Krysan, D.J. Candida albicans triggers NLRP3-mediated pyroptosis in macrophages. *Eukaryotic cell* **13**, 329–340 (2014).
50. O'Meara, T.R. *et al.* Global analysis of fungal morphology exposes mechanisms of host cell escape. *Nat Commun* **6**, 6741 (2015).
51. O'Meara, T.R. *et al.* High-Throughput Screening Identifies Genes Required for Candida albicans Induction of Macrophage Pyroptosis. *mBio* **9** (2018).
52. Shi, J. *et al.* Cleavage of GSDMD by inflammatory caspases determines pyroptotic cell death. *Nature* **526**, 660–665 (2015).
53. Kayagaki, N. *et al.* Caspase-11 cleaves gasdermin D for non-canonical inflammasome signalling. *Nature* **526**, 666–671 (2015).
54. Brown , G.D. *et al.* Dectin-1 Is A Major β-Glucan Receptor On Macrophages. *Journal of Experimental Medicine* **196**, 407–412 (2002).
55. Bugarcic, A. *et al.* Human and mouse macrophage-inducible C-type lectin (Mincle) bind Candida albicans. *Glycobiology* **18**, 679–685 (2008).
56. Wevers, Brigitte A. *et al.* Fungal Engagement of the C-Type Lectin Mincle Suppresses Dectin-1-Induced Antifungal Immunity. *Cell Host & Microbe* **15**, 494–505 (2014).
57. O'Brien, X.M. *et al.* Lectin site ligation of CR3 induces conformational changes and signaling. *The Journal of biological chemistry* **287**, 3337–3348 (2012).
58. Gow, N.A.R., van de Veerdonk, F.L., Brown, A.J.P. & Netea, M.G. Candida albicans morphogenesis and host defence: discriminating invasion from colonization. *Nature Reviews Microbiology* **10**, 112–122 (2012).
59. Gringhuis, S.I. *et al.* Dectin-1 directs T helper cell differentiation by controlling noncanonical NF-kappaB activation through Raf-1 and Syk. *Nat Immunol* **10**, 203–213 (2009).
60. Mitra, S.K. & Schlaepfer, D.D. Integrin-regulated FAK–Src signaling in normal and cancer cells. *Current Opinion in Cell Biology* **18**, 516–523 (2006).
61. Hansen, M. *et al.* Macrophage Phosphoproteome Analysis Reveals MINCLE-dependent and -independent Mycobacterial Cord Factor Signaling. *Mol Cell Proteomics* **18**, 669–685 (2019).
62. Castel, P., Toska, E., Engelman, J.A. & Scaltriti, M. The present and future of PI3K inhibitors for cancer therapy. *Nature Cancer* **2**, 587–597 (2021).
63. Mistry, J.J. *et al.* ROS-mediated PI3K activation drives mitochondrial transfer from stromal cells to hematopoietic stem cells in response to infection. *Proceedings of the National Academy of Sciences of the United States of America* **116**, 24610–24619 (2019).

64. Zheng, D. *et al.* AKT but not MYC promotes reactive oxygen species-mediated cell death in oxidative culture. *Journal of Cell Science* **133** (2020).
65. Lopez-Mejia, I.C. *et al.* Oxidative stress-induced FAK activation contributes to uterine serous carcinoma aggressiveness. *Mol Oncol* **17**, 98–118 (2023).
66. Wang, X. *et al.* IGFBP2 induces podocyte apoptosis promoted by mitochondrial damage via integrin α5/FAK in diabetic kidney disease. *Apoptosis* **29**, 1109–1125 (2024).
67. Ecker, V. *et al.* Targeted PI3K/AKT-hyperactivation induces cell death in chronic lymphocytic leukemia. *Nat Commun* **12**, 3526 (2021).
68. Luyendyk, J.P. *et al.* Genetic analysis of the role of the PI3K-Akt pathway in lipopolysaccharide-induced cytokine and tissue factor gene expression in monocytes/macrophages. *J Immunol* **180**, 4218–4226 (2008).
69. Littman, B.H., Dastvan, F.F., Carlson, P.L. & Sanders, K.M. Regulation of monocyte/macrophage C2 production and HLA-DR expression by IL-4 (BSF-1) and IFN-gamma. *J Immunol* **142**, 520–525 (1989).
70. Westermann, S. *et al.* Siglec-F Promotes IL-33-Induced Cytokine Release from Bone Marrow-Derived Eosinophils Independently of the ITIM and ITIM-like Motif Phosphorylation. *J Immunol* **208**, 732–744 (2022).
71. Zeng, J. *et al.* Stearic Acid Induces CD11c Expression in Proinflammatory Macrophages via Epidermal Fatty Acid Binding Protein. *J Immunol* **200**, 3407–3419 (2018).
72. McNally, A.K. & Anderson, J.M. Interleukin-4 induces foreign body giant cells from human monocytes/macrophages. Differential lymphokine regulation of macrophage fusion leads to morphological variants of multinucleated giant cells. *Am J Pathol* **147**, 1487–1499 (1995).
73. Verma, A.H. *et al.* Oral epithelial cells orchestrate innate type 17 responses to Candida albicans through the virulence factor candidalysin. *Sci Immunol* **2** (2017).
74. Valentine, M. *et al.* Nanobody-mediated neutralization of candidalysin prevents epithelial damage and inflammatory responses that drive vulvovaginal candidiasis pathogenesis. *mBio* **15**, e0340923 (2024).
75. Jaeger, M. *et al.* A Genome-Wide Functional Genomics Approach Identifies Susceptibility Pathways to Fungal Bloodstream Infection in Humans. *J Infect Dis* **220**, 862–872 (2019).
76. Schittenhelm, L., Hilkens, C.M. & Morrison, V.L. β(2) Integrins As Regulators of Dendritic Cell, Monocyte, and Macrophage Function. *Front Immunol* **8**, 1866 (2017).
77. Lawson, C. *et al.* FAK promotes recruitment of talin to nascent adhesions to control cell motility. *Journal of Cell Biology* **196**, 223–232 (2012).
78. Võsa, U. *et al.* Large-scale cis- and trans-eQTL analyses identify thousands of genetic loci and polygenic scores that regulate blood gene expression. *Nature Genetics* **53**, 1300–1310 (2021).
79. Warnatsch, A. *et al.* Reactive Oxygen Species Localization Programs Inflammation to Clear Microbes of Different Size. *Immunity* **46**, 421–432 (2017).
80. Lowman, D.W. *et al.* Novel structural features in Candida albicans hyphal glucan provide a basis for differential innate immune recognition of hyphae versus yeast. *The Journal of biological chemistry* **289**, 3432–3443 (2014).
81. Kashem, S.W. *et al.* Candida albicans morphology and dendritic cell subsets determine T helper cell differentiation. *Immunity* **42**, 356–366 (2015).
82. Oh, S. *et al.* Pathogen size alters C-type lectin receptor signaling in dendritic cells to influence CD4 Th9 cell differentiation. *Cell Reports* **38**, 110567 (2022).
83. Steele, C. *et al.* The beta-glucan receptor dectin-1 recognizes specific morphologies of Aspergillus fumigatus. *PLoS pathogens* **1**, e42 (2005).
84. Hurley, J.C. Antibiotic-induced release of endotoxin: a reappraisal. *Clin Infect Dis* **15**, 840–854 (1992).
85. Zhou, T. *et al.* Hyphal Als proteins act as CR3 ligands to promote immune responses against Candida albicans. *Nat Commun* **15**, 3926 (2024).
86. Hoxhaj, G. & Manning, B.D. The PI3K–AKT network at the interface of oncogenic signalling and cancer metabolism. *Nature Reviews Cancer* **20**, 74–88 (2020).

87. Dietschmann, A. *et al.* Phosphatidylinositol 3-Kinase (PI3K) Orchestrates Aspergillus fumigatus-Induced Eosinophil Activation Independently of Canonical Toll-Like Receptor (TLR)/C-Type-Lectin Receptor (CLR) Signaling. *mBio* **13**, e0123922 (2022).
88. Wüthrich, M. *et al.* Fonsecaea pedrosoi-induced Th17-cell differentiation in mice is fostered by Dectin-2 and suppressed by Mincle recognition. *European Journal of Immunology* **45**, 2542–2552 (2015).
89. Yoon, S.O. *et al.* Focal Adhesion- and IGF1R-Dependent Survival and Migratory Pathways Mediate Tumor Resistance to mTORC1/2 Inhibition. *Mol Cell* **67**, 512–527.e514 (2017).
90. Schrijver, D.P. *et al.* Resolving sepsis-induced immunoparalysis via trained immunity by targeting interleukin-4 to myeloid cells. *Nat Biomed Eng* **7**, 1097–1112 (2023).
91. Bono, C. *et al.* GM-CSF Programs Hematopoietic Stem and Progenitor Cells During Candida albicans Vaccination for Protection Against Reinfection. *Front Immunol* **12**, 790309 (2021).
92. Cheng, S.C. *et al.* mTOR- and HIF-1α-mediated aerobic glycolysis as metabolic basis for trained immunity. *Science (New York, N.Y.)* **345**, 1250684 (2014).
93. Paul, W.E. History of interleukin-4. *Cytokine* **75**, 3–7 (2015).
94. van de Laar, L., Coffer, P.J. & Woltman, A.M. Regulation of dendritic cell development by GM-CSF: molecular control and implications for immune homeostasis and therapy. *Blood* **119**, 3383–3393 (2012).
95. Nogueira, V. *et al.* Akt determines replicative senescence and oxidative or oncogenic premature senescence and sensitizes cells to oxidative apoptosis. *Cancer Cell* **14**, 458–470 (2008).
96. Lanahan, S.M., Wymann, M.P. & Lucas, C.L. The role of PI3Kγ in the immune system: new insights and translational implications. *Nature Reviews Immunology* **22**, 687–700 (2022).
97. Hynes, R.O. Integrins: Bidirectional, Allosteric Signaling Machines. *Cell* **110**, 673–687 (2002).
98. Wells, C.A. *et al.* The macrophage-inducible C-type lectin, mincle, is an essential component of the innate immune response to Candida albicans. *J Immunol* **180**, 7404–7413 (2008).
99. Dietschmann, A. *et al.* Th2-dependent disappearance and phenotypic conversion of mouse alveolar macrophages. *European Journal of Immunology* **n/a**, 2350475 (2023).
100. Lockhart, S.R., Chowdhary, A. & Gold, J.A.W. The rapid emergence of antifungal-resistant human-pathogenic fungi. *Nature Reviews Microbiology* **21**, 818–832 (2023).
101. Huang, J. *et al.* Pan-drug resistance and hypervirulence in a human fungal pathogen are enabled by mutagenesis induced by mammalian body temperature. *Nature Microbiology* **9**, 1686–1699 (2024).
102. Casadevall, A., Kontoyiannis, D.P. & Robert, V. Environmental Candida auris and the Global Warming Emergence Hypothesis. *mBio* **12**, 10.1128/mbio.00360–00321 (2021).
103. Williams, T.J., Harvey, S. & Armstrong-James, D. Immunotherapeutic approaches for fungal infections. *Current Opinion in Microbiology* **58**, 130–137 (2020).
104. Wan, L. *et al.* Effect of Granulocyte-Macrophage Colony-Stimulating Factor on Prevention and Treatment of Invasive Fungal Disease in Recipients of Allogeneic Stem-Cell Transplantation: A Prospective Multicenter Randomized Phase IV Trial. *J Clin Oncol* **33**, 3999–4006 (2015).
105. Gross, O. *et al.* Card9 controls a non-TLR signalling pathway for innate anti-fungal immunity. *Nature* **442**, 651–656 (2006).
106. Brunner, J.S. *et al.* The PI3K pathway preserves metabolic health through MARCO-dependent lipid uptake by adipose tissue macrophages. *Nat Metab* **2**, 1427–1442 (2020).
107. Tzeng, T.-C. *et al.* A Fluorescent Reporter Mouse for Inflammasome Assembly Demonstrates an Important Role for Cell-Bound and Free ASC Specks during In Vivo Infection. *Cell Reports* **16**, 571–582 (2016).
108. Sabroe, I., Jones, E.C., Whyte, M.K.B. & Dower, S.K. Regulation of human neutrophil chemokine receptor expression and function by activation of Toll-like receptors 2 and 4. *Immunology* **115**, 90–98 (2005).

109. Simard, J.C., Girard, D. & Tessier, P.A. Induction of neutrophil degranulation by S100A9 via a MAPK-dependent mechanism. *J Leukoc Biol* **87**, 905–914 (2010).
110. Schindelin, J. *et al.* Fiji: an open-source platform for biological-image analysis. *Nature Methods* **9**, 676–682 (2012).
111. Wessel, D. & Flügge, U.I. A method for the quantitative recovery of protein in dilute solution in the presence of detergents and lipids. *Analytical Biochemistry* **138**, 141–143 (1984).
112. Supek, F., Bošnjak, M., Škunca, N. & Šmuc, T. REVIGO Summarizes and Visualizes Long Lists of Gene Ontology Terms. *PLOS ONE* **6**, e21800 (2011).
113. Valentine, M. *et al.* Probiotic Lactobacillus Species Modulate Immune Responses During Vaginal Epithelial Cell Colonization. *The Journal of Infectious Diseases* (2025).
114. Wurster, S. *et al.* Live Monitoring and Analysis of Fungal Growth, Viability, and Mycelial Morphology Using the IncuCyte NeuroTrack Processing Module. *mBio* **10** (2019).
115. Chang, C.C. *et al.* Second-generation PLINK: rising to the challenge of larger and richer datasets. *Gigascience* **4**, 7 (2015).
116. Pruim, R.J. *et al.* LocusZoom: regional visualization of genome-wide association scan results. *Bioinformatics* **26**, 2336–2337 (2010).
117. Perez-Riverol, Y. *et al.* The PRIDE database resources in 2022: a hub for mass spectrometry-based proteomics evidences. *Nucleic Acids Res* **50**, D543–d552 (2022).

Supplementary Files

This is a list of supplementary files associated with this preprint. Click to download.

- SupplementaryVideo1Hyphoptosisoverview.mp4
- SupplementaryVideo2HyphoptosisZoomedIn.mp4
- SupplementaryVideo3HyphoptosiswithGiantcells.mp4